
Helical Multidetector Chest CT

Pilar García-Peña, Tom A. Watson, and Catherine M. Owens

Contents

1	Introduction	75
2	Technical Considerations	76
2.1	Helical Technique.....	76
2.2	Personnel and Environment Requirements.....	79
2.3	Previous Exam Evaluation.....	79
2.4	Preparation of the Patient: Fasting Requirements.....	80
2.5	Immobilization and Other Practical Tips.....	80
2.6	Breath-Holding Information.....	80
2.7	Sedation.....	80
2.8	Intravenous Contrast Material Administration.....	83
2.9	Technical Parameters and Protocols.....	86
2.10	Image Postprocessing.....	89
2.11	Newer Advances in CT.....	95
3	Helical Chest CT Main Applications	98
3.1	Evaluation of Pulmonary Nodules and Chest Masses.....	99
3.2	Evaluation of Vascular Anatomy: CT Angiography.....	101
3.3	Evaluation of Central Airways.....	104
3.4	Evaluation of Difficult Areas: Cervicothoracic Junction, Peridiaphragmatic Area, and Chest Wall.....	106
3.5	Evaluation of Critically Ill Patients.....	106
3.6	Evaluation of Inconclusive Images on Chest Radiography.....	106
4	Conclusions	106
	References	107

Abstract

There has been a revolution in the technology of helical computed tomography, with increased speed of acquisition of the CT examinations, improvements in image quality, reduction in volume of intravenous contrast material required and a significant reduction in the need for sedation. All of these technological improvements have particular clinical benefits for children. Indeed many of the significant advances in CT technology are invaluable when studying the airways and cardiovascular structures. These improvements in CT angiography, with consequent isotropic resolution, allow excellent quality multiplanar reconstructions, with holographic three-dimensional reformatted images, available to clinicians that will facilitate best clinical diagnostic and surgical planning. The positive benefits of CT must be considered in the light of potential radiation exposure risks. We are obliged to produce low-dose, weight-based paediatric protocols, which are optimised to provide images that are ‘fit for diagnostic purpose’. We use this chapter as an opportunity to outline the technical aspects of helical MDCT technique, the many potential clinical indications where thoracic CT may benefit children, and we suggest protocols which may be used in children—a very precious commodity!

P. García-Peña (✉)
Professor Emeritus in Paediatric Radiology,
Department of Paediatric Radiology, Vall d’Hebron Hospitals,
Ps. Vall d’Hebron 119–129, 08035 Barcelona, Spain
e-mail: plgarciapeña@gmail.com

T. A. Watson
Department of Paediatric Radiology,
Great Ormond Street Hospital for Children,
NHS Trust, Great Ormond Street, London, WC1N 3JH, UK

C. M. Owens
Department of Cardiorespiratory Radiology,
Great Ormond Street Hospital for Children,
NHS Trust, Great Ormond Street, London, WC1N 3JH, UK

1 Introduction

There has been much (adverse) publicity over the last decade regarding the use of computed tomography in the medical setting (Brenner and Hall 2007), which has raised public awareness on a global scale. This has resulted in an increased public interest in the importance of justification of computed tomography (CT) by the referring clinical teams. It is important to perform a risk benefit analysis at this time, and to assess whether CT is the only modality that can answer the clinical question posed. Other modalities such as MRI or US

can be used in the abdomen and pelvis, but chest CT is still the preferred choice for imaging lung parenchymal disease.

Once CT has been deemed the most appropriate test, the radiology team must optimize the CT technique so that the best quality images (which are “fit for diagnostic purpose”) are acquired at as low a radiation dose as is possible (García-Peña and Lucaya 1999). This will follow the ALARA, i.e., As Low as is Reasonably Achievable principle.

With this in mind we set out to address important issues, which will help to address the current status of chest CT and its importance in clinical practice and also to provide tips and tricks to enhance image quality via optimization of acquisition and prudent use of post-processing techniques.

Computed tomography in children poses a set of unique problems that are not encountered in adults. The relative lack of visceral fat combined with motion inherent to the small child, (cardiac respiratory and otherwise) results in degradation of image quality, making the recognition of normal anatomical structures and some pathologies more difficult.

The recent major advances in technology, in conjunction with meticulous attention paid to CT technique, and enhanced training of radiologists and technicians have all combined together to improve the sensitivity and specificity of pediatric CT imaging, and have resulted in more precise diagnostic possibilities.

The introduction of helical CT, and more specifically, multidetector CT (MDCT), has further increased the utility, and hence extended the indications for CT in the evaluation of pediatric patients.

Many of the significant changes in current diagnostic practice are solely related to the introduction of helical CT technology and MDCT, which have enabled the study of airway and vascular structures, the development of CT angiography and virtual endoscopy, and improvements in the quality of multiplanar reconstructions.

Helical CT technology has demonstrated real and significant benefits for pediatric patients.

The use of IV contrast agents can be optimized, sedation rates reduced, and radiation exposure to the patient can be decreased, by using extended pitch and by eliminating the need to rescan nondiagnostic data.

MDCT radiation doses can be significantly reduced using custom designed, in-house modification of manufacturers’ protocols, balancing adequate signal-to-noise ratio with diagnostic image quality which are “fit for diagnostic purpose.”

MDCT also improves the overall image quality of two- and three-dimensional (2D and 3D) reconstructions, an important factor when analyzing specific diseases in children.

2 Technical Considerations

2.1 Helical Technique

In contrast to conventional CT, which is based on the collection of data from sequential scans, helical CT data is obtained continuously during table motion and results in a volumetric acquisition of scan data. If direct reconstruction were performed on these data the resulting images would be of poor quality, being compromised by motion artifacts.

Thus, to compensate for the problems induced by table motion, the image data is interpolated prior to reconstruction (Brink et al. 1994b; Brink 1995; Napel 1995; Siegel and Luker 1995; Siegel 2003).

When compared to conventional section-by-section CT, helical CT has a number of advantages in the examination of pediatric patients. By using the reconstruction capabilities of helical CT we can obtain overlapping slices, a fact that improves lesion depiction without increasing radiation exposure. Post processing of overlapping slices provides high-quality 2D and 3D images, extending the diagnostic applications.

Fortunately in children, due to the possibility of very thin data acquisition with MDCT equipment, it is usually unnecessary to use overlapping slices to obtain a better quality of image for reconstruction.

As a result of isotropic data set acquisition image reconstruction can be performed along any slice using z-axis interval scanning (Singh et al. 2012).

The very short scanning times allow more precise temporal delivery of contrast medium and as a result, contrast-enhanced studies can be performed during peak vascular enhancement. This also may allow a reduction of at least 25 % in the volume of contrast agent needed (Costello et al. 1992a).

As the speed of scanning a particular anatomic area is determined by the collimation thickness and the pitch (defined as the ratio of the table speed, expressed in millimeters per second to collimation thickness, expressed in millimeters multiplied by the time to acquire 360° of data), shorter scan times may help to eliminate or decrease motion artifacts (Rubin et al. 1998).

Some MDCT equipment, instead of using the pitch concept, use the table feed concept expressed in millimeters (millimeters that table moves after each acquisition). High-speed acquisition allows high-quality 2D and 3D image reconstruction and decreases the need for sedation (a very important consideration in pediatric patients).

Radiation dose can be reduced in helical scanning without compromising diagnostic image quality (Takahashi et al. 1998). This is more pertinent, as children are relatively more radiosensitive than adults and have a longer life span in which to manifest radiation-related disease.

Radiation dose is a contentious issue in pediatrics. It is claimed that high cumulative radiation doses may be associated with an increased lifetime risk of brain tumors (Pearce et al. 2012).

As proposed by the ALARA “as low as reasonably achievable” principle, the selection of appropriate scanning parameters focuses on the optimization of image quality, while delivering the lowest possible radiation dose and shifting the risk–benefit balance toward benefit (Shrimpton and Edyream 1998; Callahan 1998; Paterson et al. 2001; Oddone et al. 2005).

The various technical parameters that need to be selected for any scan include: thickness of collimation, tube current—milliamperage and kilovoltage.

The thickness of collimation is the minimum section thickness that can be acquired once the scan is finished and in a 64-row MDCT scanner is 0.6 mm. (See Tables 1, 2, and 3).

The axial images are reconstructed at 1 mm and archived to the PACS system within our hospitals. In recent years, we have made efforts to standardize low-dose protocols for the children scanned in our institution, and the currently applied parameters are summarized in the Tables 1, 2, 3, and 4.

Methods adopted to minimize radiation dose in MDCT are multiple.

Automatic exposure control (AEC)

This system focuses on the average amount of noise per slice seen as acceptable and “fit for diagnostic purpose” by the user. The mAs is adjusted accordingly and can result in significant dose reduction (that is when the mAs can be reduced).

Automated tube current modulation systems have been produced by all of the major MDCT scanner manufacturers (Greess et al. 2004).

The tube current is modified to follow the anatomy of the patient, maintaining the same noise level within the images acquired.

Two methods are available, modulation in the x- and y-axes (angular modulation) and z-axis modulation.

Angular modulation adjusts the tube current, while the X-ray tube passes around the patient’s body, e.g., in an adult the mAs is reduced in the AP versus the lateral position. This is more beneficial in older patients who may be wider in the side to side, compared to anteroposterior directions, whereas baby’s bodies are more spherical.

In adults, effective doses can be reduced by up to 30 % (Greess et al. 2002, 2004).

Radiation dose reduction in CT examinations of children can be achieved by an attenuation-based on-line modulation of tube current (CARE dose) (Greess et al. 2002).

Table 1 Protocol: Chest survey

Standard chest CT (‘combiscan’)	
Scan mode	Helical
Indication	CVS anomalies
	Strictures and small tracheobronchial stenoses
	Peripheral airways disease
	Tracheomalacia
	Tumors and metastases
Anatomic coverage	Congenital lung abnormalities
	Thoracic inlet to diaphragm
	The upper abdomen is included if sequestration is suspected
Tube collimation	0.6 mm
Tube rotation	0.5 s
Slice reconstruction	1 mm
Pitch	1
Scan parameters	1–9 kg—80 kV, 60 QmAs, CTDIvol 0.88 mGy
	10–15 kg—100 kV, 30 QmAs, CTDIvol 1.0 mGy
	16–25 kg—100 kV, 38 QmAs, CTDIvol 1.26 mGy
	26–35 kg—100 kV, 42 QmAs, CTDIvol 1.4 mGy
	36–45 kg—100 kV, 48 QmAs, CTDIvol 1.6 mGy
	Over 46 kg—100 kV, 55 QmAs, CTDIvol 1.83 mGy
Intravenous contrast	2 mls/kg (max 100 ml)
	Scan delay of 20–30 s from start of injection depending on patient weight
Reconstruction kernels	B30f 1 mm (mediastinal window)
	B60f 1 mm (lung window)
Tube current modulation	On

Imaging of the pediatric chest with a 64-row MDCT scanner

This **z-axis current modulation** needs the selection of an acceptable noise level and a maximum and minimum tube current, which are chosen before the examination. Thence, the scanner can adjust the tube current within the selected range and maintain the noise level, using data from the scout view or during gantry rotation. The reduction in tube current can be around 40 % using this technique (Karla et al. 2004).

However, the choice of tube current must be accurate prior to the examination as the automated dose control is set to preferentially overexpose to ensure good quality images and may in fact result in a dose increase (Gudjónsdóttir et al. 2010).

Table 2 Protocol: HRCT chest scanning parameters on a 64 slice system

HRCT	
Scan mode	Sequential
Scan parameter	100 kVp
	1–25 kg—30 QmAs, CTDIvol 0.18 mGy
	26–35 kg—35 QmAs, CTDIvol 0.21 mGy
	36–50 kg—42 QmAs, CTDIvol 0.25 mGy
	Over 50 kg—60 QmAs, CTDIvol 0.36 mGy
Tube rotation time	0.5 s
Tube collimation	2 × 1 mm
Table feed	Inspiration—10 mm
	Expiration—25–35 mm dependent on size of child
Coverage	Inspiration—apices to base of lungs
	Expiration—3 evenly spaced slices to cover upper/middle/lower lobes
	Nonbreath-hold—2 slices each in R & L decubitus position
Tube current modulation	On
Recon slice width	1 mm
Recon Kernel	1st recon—B60
	2nd recon—B30
Window width/level	1st recon—high-resolution lung parenchyma setting
	2nd recon—mediastinum setting
Contrast media	–
Scan delay	–

Reduction of the kilovoltage to 100 kVp when imaging the thorax

Further reduction to 80 kVp is possible for CT Angiography, but as resolution of the lung parenchyma is not always ideal (especially when looking for subtle patterns of interstitial lung disease) the 80 kVp option is applied only if lung pathology is unlikely and vascular anatomy is of paramount importance.

Iterative reconstruction

One of the most important advances in CT technique has been the development and utilization of new iterative reconstruction techniques which have resulted in a dramatic reduction in CT examination dose (Silva et al. 2010).

Iterative reconstruction techniques attempt to accurately rebuild images by focusing on noise reduction. One type of iterative reconstruction technique, Adaptive Statistical Iterative reconstruction (ASIR), uses information obtained from the Filtered Back Projection (FBP) algorithm as an initial building block for image reconstruction. The ASIR

Table 3 Protocol: CT angiography scanning parameters on a 64 slice system

CT Angiography	
Scan mode	Helical
Scan parameter	1–15 kg—80 kV, 60 QmAs, CTDIvol 0.88 mGy
	16–25 kg—100 kV, 30 QmAs, CTDIvol 1.0 mGy
	26–35 kg—100 kV, 36 QmAs, CTDIvol 1.2 mGy
	36–45 kg—100 kV, 45 QmAs, CTDIvol 1.5 mGy
	46–55 kg—100 kV, 52 QmAs, CTDIvol 1.7 mGy
	Over 56 kg—100 kV, 62 QmAs, CTDIvol 2.1 mGy
Tube rotation	0.5 s
Tube collimation	64 × 0.6 mm
Pitch	1
Coverage	Dependent on indication
Tube current modulation	On
Recon slice width	1 mm
Recon Kernel	1st recon—B30
	2nd recon—B60
Window width/level	1st recon—medium soft, mediastinum
	2nd recon—high-resolution for lung parenchyma
Contrast media	2 mL/kg to maximum 150 mL
Scan delay	Bolus tracked—ROI outside body

model then uses matrix algebra to transform the measured value of each pixel (y) to a new estimate of the pixel value (y'). This pixel value is then compared with the ideal value that the noise model predicts. The process is repeated in successive iterative steps until the final estimated and ideal pixel values ultimately converge.

Using this method, ASIR is able to selectively identify and then subtract noise from an image. Thus, ASIR reconstructs images with lower image noise compared with FBP.

When there are specific clinical indications, for example when high-contrast lesions are surrounded by low-contrast structures, dedicated low-dose protocols have been routinely used in the past in an effort to minimize radiation dose. For example, studies have suggested that low-dose CT is adequate for CT colonography (Cohnen et al. 2004), pulmonary CT angiography, and tracheobronchial evaluation (Heyer et al. 2007).

It is important to remember that although satisfactory for the dedicated evaluation of the intended specific anatomy,

Table 4 Dose comparison for different scanning protocols, based on actual patient data from GOSH

Effective dose per study (mSv)					
	Standard chest	HRCT	CTA	CXR	
<15 kg	1.6	0.4	1	0.00487	0.00799
<25 kg	1.5	0.4	1.9	0.00874	0.01086
<35 kg	2.2	0.6	2.6	0.01163	0.00968
35–44 kg	2.5	1.1	2.8	0.01769	0.01452

these protocols were implemented by knowing that image quality would be significantly reduced outside the immediate area of interest.

The application of the ASIR algorithm to these low-dose studies can significantly reduce image noise and improve overall image quality when compared with low-dose standard FBP techniques.

Pitch

Unlike the helical single-row scanner, an increase or decrease in table feed on the MDCT scanner only affects the overall scanning time when Automated Exposure Control is enabled. The tube current is automatically compensated to ensure that the present effective and total mAs is delivered. In other words, an increase in table speed triggers a concomitant increase in mA and this has no impact on the effective dose delivered.

Anatomical coverage for imaging of the pediatric thorax extends from the thoracic inlet to the diaphragm, but a greater degree of coverage may be warranted in certain clinical cases, such as an extralobar pulmonary sequestration, that may be present in the upper abdominal cavity.

In order to increase spatial resolution, the **field of view (FOV)** should closely approximate the cross-sectional area of the body part being studied. A large FOV would result in waste of matrix space and partial volume averaging would generate poor quality images (Callahan 1998).

Helical equipment is remarkably silent as compared to conventional scanners. For this reason, pediatric patients are not usually frightened and remain calm and still. This in itself reduces the need for sedation and improves image quality.

The quality of multiplanar reformatted images, MPR (coronal, sagittal, and curved) and 3D images is significantly improved with MDCT, which decreases motion-related artifacts and provides a smoothing effect of overlapped image reconstruction or due to the thin collimation of the new equipment, reducing stair-step artifacts. Such 3D images can be optimally rotated to display specific normal and abnormal structures allowing analysis of selected parts.

2.1.1 Limitations and Disadvantages of Helical CT Technique

The technical limitations previously associated with Helical CT technology have been rendered largely obsolete. The new generation of helical MDCT scanners provides a vast

improvement in volume coverage speed with better resulting diagnostic image quality (Hu et al. 2000).

2.1.2 Pitfalls of Helical CT Technique

A common technical artifact associated with traditional helical data acquisition is the stair-step artifact (Wang and Vannier 1994). These occur along high-contrast interfaces that are oriented obliquely to the direction of patient travel. Stair casing causes the edges of longitudinally oriented structures to appear as steps rather than as straight lines. The thinner slice acquisition with MDCT scanners minimizes this technical artifact and image reconstructions are now very smooth and of very high-quality, the more detectors available the better the quality of the image.

Another potential pitfall with MDCT is related to commencing scanning before optimal organ or vessel enhancement by the contrast agent occurs in homogeneous fashion (Sillverman et al. 1995). These flow artifacts, caused by the mixing of contrast material and nonopacified blood are much more frequent in abdominal studies than in chest CT, in part because the circulation of blood is faster in the chest compared with abdominal blood circulation.

2.2 Personnel and Environment Requirements

The optimal team for performing pediatric MDCT includes a pediatric radiologist, a technician and a nurse trained in pediatric care. It is important to ensure an optimal environment for pediatric patients in the scanning area and every effort should be made to create a warm welcoming atmosphere that minimizes patient and parental anxiety. Soft lighting, toys, a quiet room decorated with children in mind, and the presence of a relative can help to comfort and console a child.

It is essential to have immediate access to a resuscitation cart with appropriate drugs and equipment for pediatric patients of all ages.

2.3 Previous Exam Evaluation

It is mandatory to check the patient's clinical records and all available previous imaging studies before performing a helical CT scan. This helps to decide if the indication is correct and allows the exam to be tailored to the specific requirements of the patient. It is particularly important with regard to the need for sedation and IV contrast administration. Careful planning can prevent difficulties during the study and minimize the potential for unanswered questions afterward. The radiologist/radiographer should explain all aspects of the procedure and the objectives of the study to the parents before obtaining parental consent. At our institution, outpatients are contacted by the nursing team prior to the scan date to assess the needs of each patient, i.e., sedation requirements, etc.

2.4 Preparation of the Patient: Fasting Requirements

The patients, parents, and nursing staffs should be informed of fasting requirements before the day of the procedure. Sometimes, no preparation is required (e.g., when studying pulmonary metastasis). When children need sedation during the examination, standard fasting regimens are similar to those for a general anesthetic, water or breast milk can be given up to 2 h prior to sedation, and food up to 4 h beforehand.

2.5 Immobilization and Other Practical Tips

Sandbags, adhesive bandages, or blankets wrapped around the patient can all be used to immobilize the patient. It is advisable to wrap a lead apron around the child in the regions adjacent to those to be scanned. This protects them from scattered radiation and, at the same time, can help to immobilize the patient. Overlying radio protective bismuth latex can be placed on breasts and thyroid gland to minimize local radiation absorption to these radiosensitive tissues. However, it should be noted that the use of these devices can increase the overall mAs with some scanners if automatic dose modulation is used and therefore increase overall dose. There is evidence to suggest that performing an initial scout view without shielding prevents the scanner increasing the dose (Coursey et al. 2008).

Toys hanging from the gantry and films or image projection on the gantry can be used to attract the attention of the child and help to keep them quiet. A system for maintaining body temperature such as warming lamps or heating blankets should be used in infants.

2.6 Breath-Holding Information

Children under 6 years of age who cannot follow breath-holding commands are examined under normal quiet breathing. In this age group, attempts at breath holding usually result in exams severely compromised by artifacts. Older children are carefully instructed in breath holding before the study.

2.7 Sedation

Helical CT and MDCT have reduced the need for sedation (White 1995; Kaste et al. 1997; Sacchetti et al. 2005). Since the introduction of silent helical CT and high-speed MDCT in our institutions, our overall rate of sedation is only 1 % of patients for MDCT versus 18 % for our previous

Table 5 Protocol: Suggested delay times from the injection of contrast medium

	Manual injection	Pressure injector
Scan initiation time delay	Immediately from termination of injection	20–30 s from start of injection. If a central line is used, this time will be reduced. Bolus tracked studies are operator dependent
Flow rate		1.5–2 ml/s
Age range	All age groups	All age groups

Table 6 Protocol: Rate of contrast media injection depending on catheter or needle gauge

Catheter/Cannula		Needle	
Gauge (g)	Flow rate (ml/s)	Gauge (g)	Flow rate (ml/s)
26	1.0	25	0.5
24	2.0	23	0.5–0.8
22	3.0	21	0.8–2.0
20	4.0	19	2.0–4.0

conventional CT studies. In 2012, using new generation CT equipments, we performed only 1 % of our thoracic CT studies with sedation.

Previously, in patients under the age of 6 years, 50 % required sedation with conventional CT and only 8 % with helical CT and 2 % with MDCT. Among the patients in this age group who needed IV contrast, 77 % had to be sedated with conventional CT, only 18 % with single slice helical CT and 3 % with MDCT. Finally, among those who did not need IV contrast material, 24 % required sedation with conventional CT, only 2 % with helical CT and 1 % with MDCT. We believe that the relative silence of the helical equipment and the high speed of acquisition have determined this reduced need for sedation. It has been widely reported that with multidetector CT the rate of sedation can be reduced (Pappas et al. 2000).

In outpatients, the need for sedation is assessed by the clinician prior to the investigation and by a dedicated nursing sedation team who telephone the parents prior to admission. A standardized questionnaire is used to evaluate the need for potential sedation.

Despite this, there will still be a need for a final sedation assessment once inside the gantry.

In our experience, infants less than 3 months of age can be successfully imaged after normal feeding and swaddling. Sleep deprivation, the night before the examination has proven to be of no benefit in either decreasing the dose of sedative drugs, or the number of sedation procedures, and can be disruptive for patients and parents.

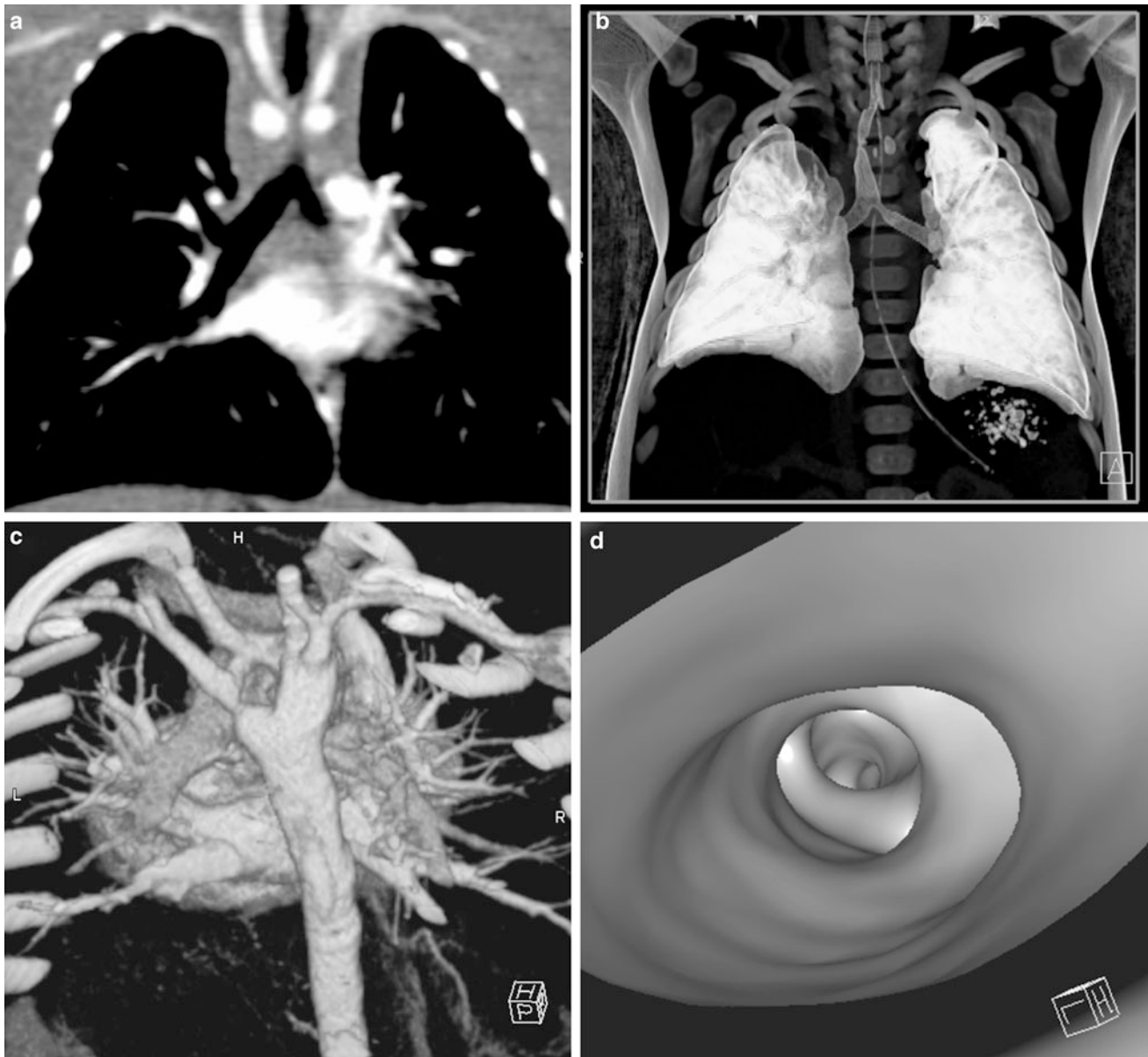


Fig. 1 Post-processing techniques. **a** Multi-planar reformats (MPR). MPR initially in coronal and sagittal planes should be the initial post-processing technique: with pixel isotropy, no information is lost, and the reformatted plane often gives a better depiction of the anatomical relationships. The coronal image shows a double aortic arch and its effect on the airway. **b** Multiplanar volume reconstructions (MPVRs). MPVRs combine volume rendered images with multi-planar imaging to produce 3D 'slabs' of the area of interest. By applying a minimal intensity projection technique a view of the airways can be produced such as this example of a congenital tracheal and left main bronchial stenosis in a 3-year-old boy with bronchiolitis. This technique is sometimes referred to as a "virtual bronchogram". Historic stair-step artefact in traditional single slice volume-rendered image (bronchographic anteroposterior

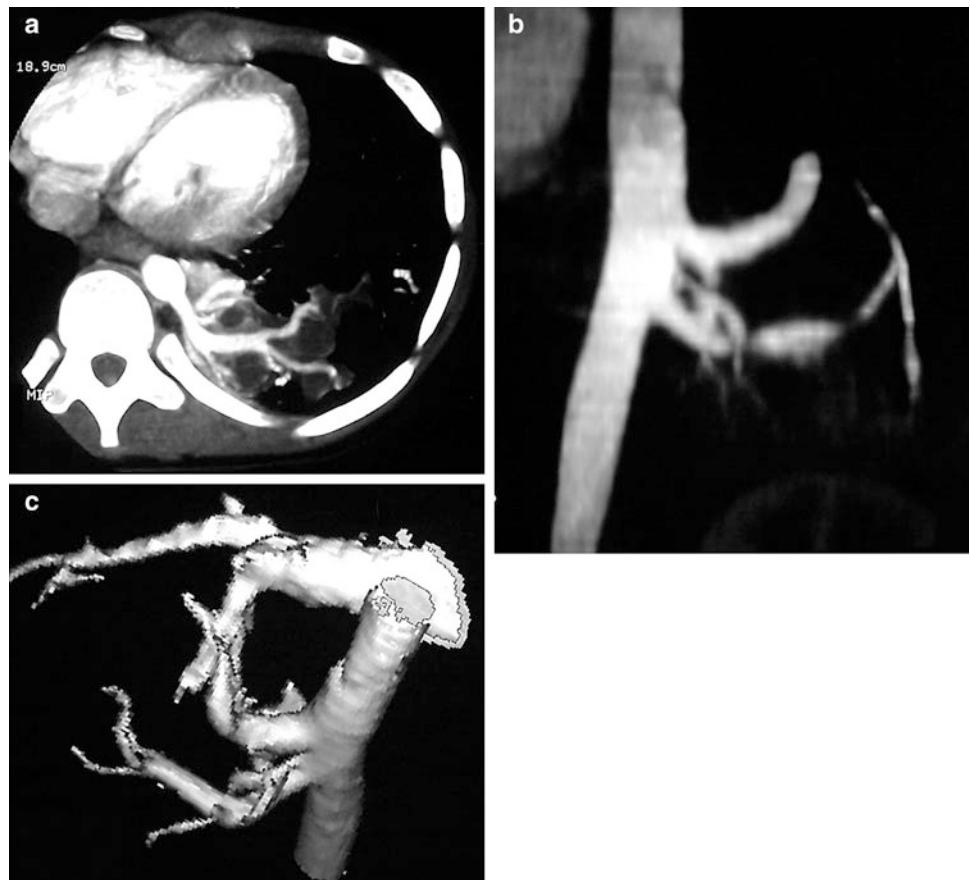
view). The artefact occurs along the left bronchus, which is oriented obliquely to the direction of patient travel during data acquisition. **c** Three-dimensional (3D) volume rendering (VR) is an excellent technique for giving an overview of complex vascular anatomy. This example, image weighted on SSD technique is a posterior view of the great vessels with the spine and posterior ribs 'cut-away', showing a double aortic arch with a dominant right arch. **d** Virtual bronchoscopy is a supplementary volume rendering technique that produces images simulating the view from fiberoptic bronchoscopy. The point of view is placed in the airway. This example demonstrates complete tracheal rings in congenital tracheal stenosis: note the abnormally rounded shape to the airway, which is normally ovoid

Before performing an examination with the use of sedation, the radiologist must decide whether benefits outweigh the potential associated risks, and verify that fasting requirements have been observed. In our institution, informed

consent for sedation is covered by the standard consent for admission and CT scan examination.

There are several contraindications to the use of sedation at our institution. These include: raised intracranial pressure,

Fig. 2 CT angiography of a pulmonary sequestration in a 6-year-old boy who was asymptomatic, but had a persistent dense image in the left pulmonary base. **a** Axial CT image. A large vessel is seen arising from the aorta, with multiple branches supplying a pulmonary mass. **b** Anteroposterior maximum intensity projection image. Three systemic vessels coming from the aorta are seen to feed the pulmonary sequestration. **c** Posteroanterior shaded surface display (SSD) image. The 3D depth perception created by SSD technique improves recognition of spatial relationships of the three vessels arising from the aorta. Two veins are also shown in the upper area of the image. With a cine-loop rotating image, the origin and the course of vessels can be better depicted



airway obstruction, gastroesophageal reflux with aspiration risk, and severe renal/hepatic failure.

We do not sedate children under 45 weeks gestation, and a “feed and wrap” protocol is usually sufficient at this age.

In children older than 45 weeks gestation but under 15 kgs we use oral Chloral Hydrate at a dose of 50 mg/kg (to a maximum dose 2000 mg).

When using this regimen and if IV contrast injection is contemplated, the intravenous line is placed in the preparation room before the patient is brought to the CT unit.

In our hospital in Spain, patients of 18 months of age and older, who need sedation, are given intravenous sodium pentobarbital, 6 mg/kg to a maximum dose of 200 mg, diluted in 10 ml saline. The syringe containing the sedation must be appropriately labeled with the drug name. A dose of 2–3 mg/kg should be given initially as slow bolus over 1–2 min. In most children, this dose is adequate and they will fall asleep within the next 4–5 min. If not, an additional dose of 2–3 mg/kg may be given. If the patient still remains awake an additional dose of 2 mg/kg can be given some 30 min later. However, this is rarely necessary. Occasionally, in some patients over 6 months of age who need IV contrast, sodium pentobarbital in the above-mentioned doses is used.

Sedation Protocol GOSH: (February 2012): Great Ormond Street Hospital for Children, London UK.

<45 weeks gestation—Feed and wrap only. No sedation.

>45 weeks gestation but <15 kgs—50 mg/kg Oral Chloral Hydrate.

Intravenous “top ups”

If the sedation is not effective, supplementary sedation may only be given by a doctor who is skilled in pediatric resuscitation according to the anesthesiologists practice and expertise, which will vary locally.

Intravenous midazolam is used at incremental doses of 100 µg/kg in children under 20 kgs. The dose must not exceed 300 µg/kg or 10 mg.

NB sedation will sometimes fail and these doses must not be exceeded.

If sedation fails, an anesthesia service must be booked for another day.

Every child undergoing sedation in the CT suite should receive oxygen and be monitored during and after the examination.

Pediatric sedation techniques have been extensively described in the literature (Cook et al. 1992; Frush et al. 1996; Egelhoff et al. 1997).

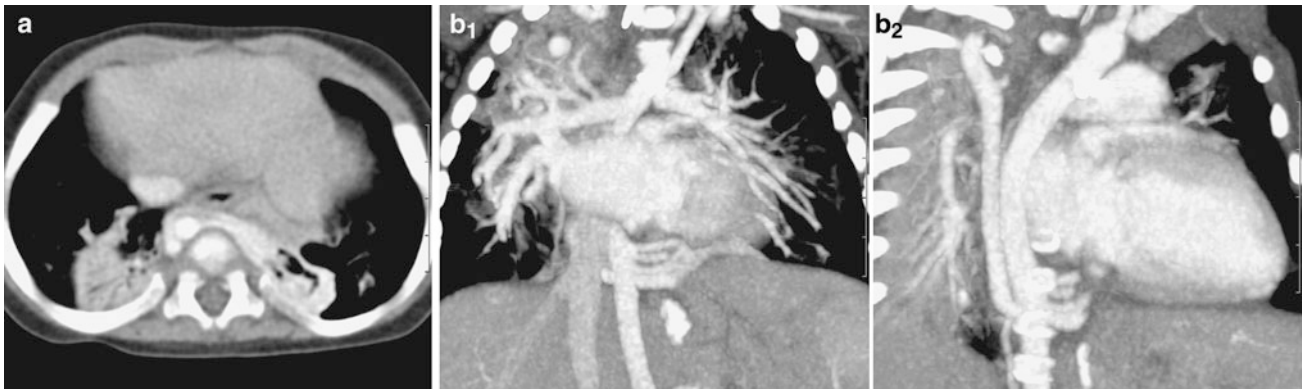


Fig. 3 Left lower lobe extralobar sequestration in a 10-month old with multiple congenital abnormalities. **a** Axial CT maximum-intensity projection images shows a large artery arising from the aorta, supplying a L lower lobe pulmonary mass. **b** Anteroposterior

(**b₁**) and sagittal oblique (**b₂**) maximum intensity projection images show three systemic vessels arising from the aorta to feed the pulmonary sequestration, which drains into the azygous (systemic venous) system

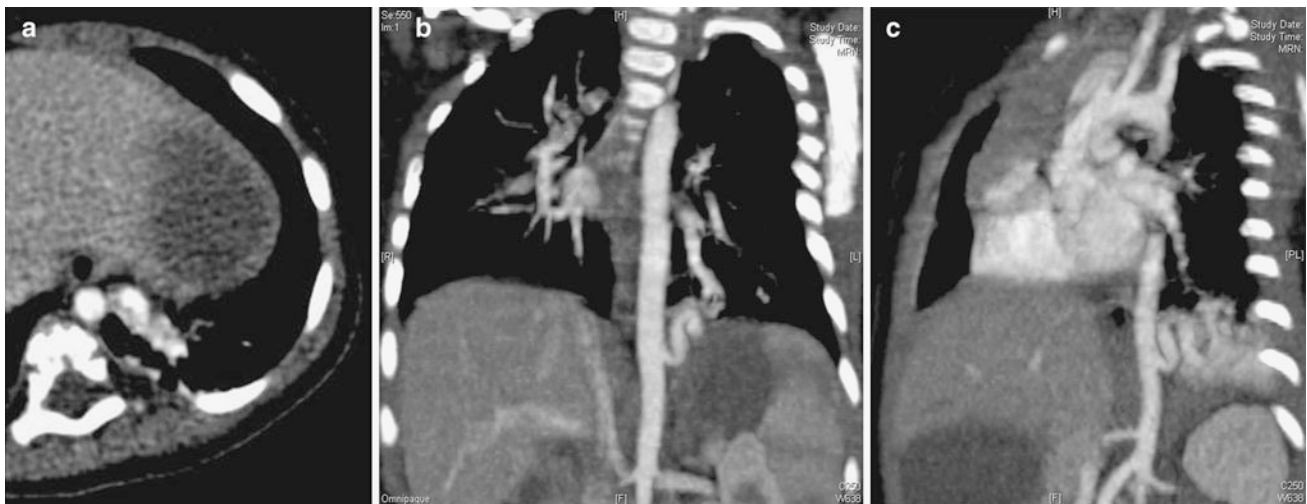


Fig. 4 Intralobar pulmonary sequestration in a 6-month-old boy. **a** Enhanced axial CT shows a difficult-to-assess lesion in the left lower lobe. **b** and **c** Oblique MIP images better depict the lesion as an

intralobar sequestration with a looping feeding vessel from the aorta and venous drainage to the inferior pulmonary vein

2.8 Intravenous Contrast Material Administration

Intravenous administration of a bolus of contrast material for helical CT studies in children can be more complicated than in adults, because of the greater variations in vessel and patient size in the pediatric population. Dosage is based on the patient's body weight. Contrast material is administered by hand or power injector, depending on these variations (Kaste and Young 1996; Frush et al. 1997). To avoid the artifact caused by contrast in the axillary vein just after the injection, the syringe is placed vertically downward and filled with contrast first and then saline solution. Since saline is less dense than contrast material, it will remain in the syringe until

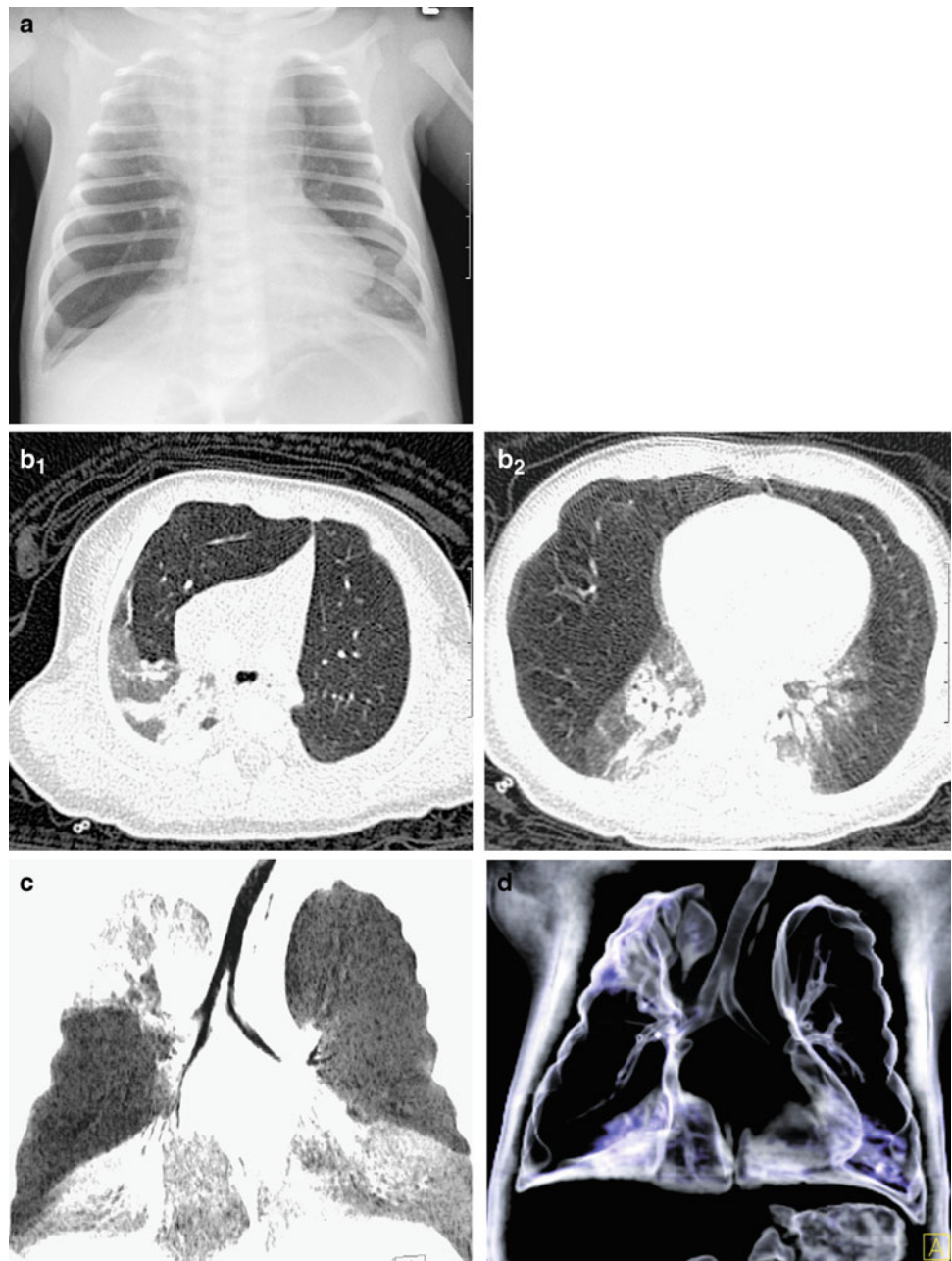
the end of the injection and then flush the vein free of contrast. This will help to obtain better images (Hopper et al. 2000).

Newer power injectors have a double system of syringes, one syringe for contrast material, and a second syringe for saline solution.

Usually, the double power injector is programmed to inject the contrast material first followed by 5–10 cc of saline solution. It is necessary to check that the venous line is functioning prior to contrast media injection to prevent extravasation occurring.

If contrast material is to be given, an intravenous catheter or a butterfly needle should be placed before the child arrives in the CT suite. This will avoid the distress associated with venepuncture performed immediately before

Fig. 5 Congenital lobar overinflation. **a** CXR. **b** (**b₁** and **b₂**) Axial CT images performed on high resolution (bony algorithm) show the attenuated, over-expanded lung in the right middle and left upper lobes, causing significant overdistension of the hemithorax. This is more easily perceived on the coronal MinIPs (**c**) and coronal VRTs (**d**) confirming the findings in a bronchographic fashion



scanning begins, and help to reduce the need for sedation. Local topical analgesics, such as lidocaine cream, can be applied to the intended venepuncture site to minimize the pain from cannula placement.

Usually, we use catheters 20–26 Gauge, permitting injection rates of 4.0–1.0 ml/s. Butterfly needles 19–25 Gauge, which give injection rates of 4.0–0.5 ml/s can also be used. (Tables 5 and 6).

One should always use the largest cannula suitable for each patient, though rates as low as 0.5–1.0 ml/s in children can still result in excellent enhanced studies. If the patient

already has a central intravenous line in situ, it should be used to gain venous access, using aseptic technique.

Nonionic, low- (240 mg of iodine per milliliter), or high- (300 mg of iodine per milliliter) osmolar contrast media can be used for CT examinations in children (Stokberger et al. 1998). In our practice, we use 240 mg/ml in infants and 300 mg/ml in older children.

The usual dose of contrast media is 1–3 ml/kg, to a maximum dose of 100 ml. In newborns the dose used is 2–3 ml/kg, in infants 2 ml/kg, in children 1.5 ml/kg, and in adolescents 1 ml/kg.

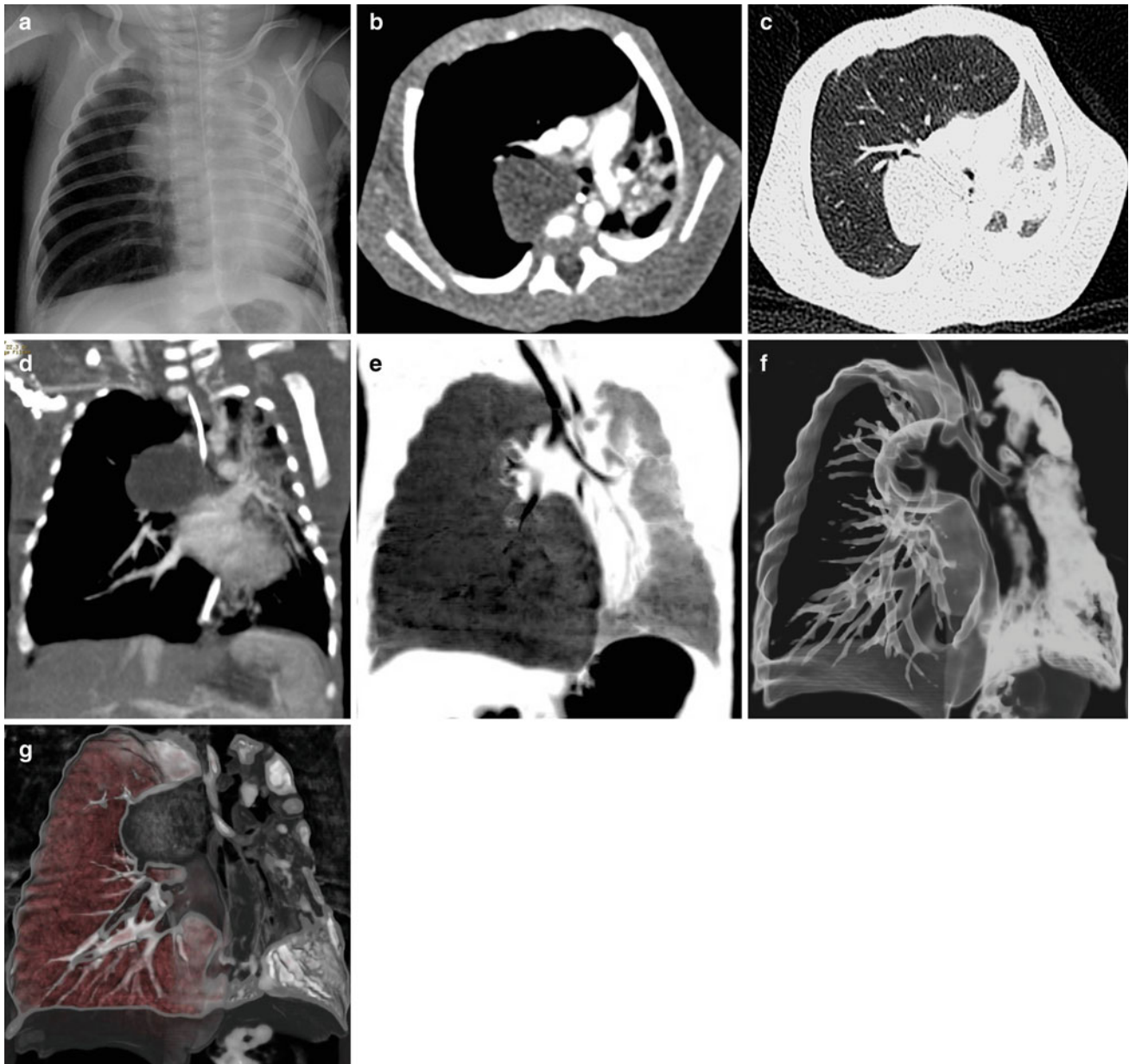


Fig. 6 Lung over-inflation secondary to an obstructive bronchogenic cyst. One-month-old boy with respiratory distress **a** On chest X-ray, there is over-inflation of the right lung with mediastinal displacement to the opposite side. A mediastinal mass can be seen on the right side. **b** Enhanced axial CT shows a hypodense mediastinal mass on the right side, with substantial over-inflation of the right lung, and mediastinal and lung displacement to the left side. **c** Axial CT B60f for high-resolution

lung parenchyma detail shows right lung over-inflation secondary to right bronchus compression, and left lung atelectasis. **d** Coronal MPR depicts the hypodense mass and mediastinal displacement with lung atelectasis. **e** Coronal MinIP shows right lung over-inflation and right main bronchus compression. This is the best technique to evaluate the central airways and lung attenuation. **f** and **g** VR images of the bronchogram and mediastinum show similar findings

In our experience, helical CT has allowed a 20 % reduction in the volume of intravenous contrast medium given when compared to conventional CT. Similar findings have been described in the literature (Costello et al. 1992a). Optimal contrast enhancement during helical scanning depends on careful selection of the appropriate time of

scanning, as well as on choosing the precise amount of contrast material and the optimal injection rate. The rate of injection depends on the needle or catheter size (Table 6). The timing of the onset of scanning is a crucial factor in successful imaging, but is also one of the trickiest aspects of performing pediatric helical CT.

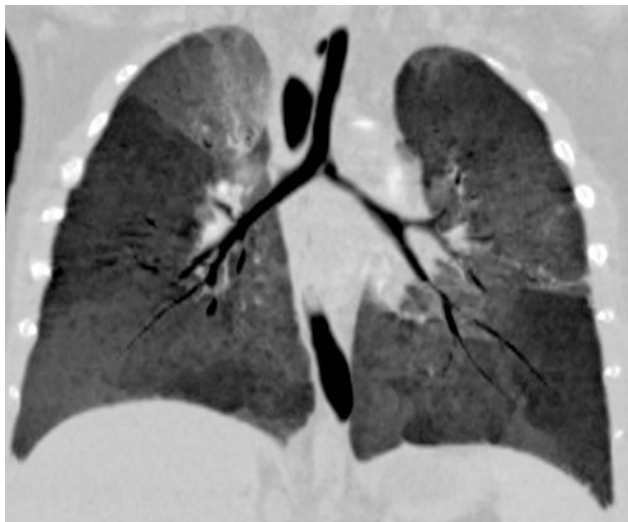


Fig. 7 Small airway disease in constrictive obliterative bronchiolitis in a 2-year-old boy. Coronal MinIP is a good technique to demonstrate the heterogeneous attenuation of both lungs

2.9 Technical Parameters and Protocols

Helical CT has essentially replaced conventional CT for examinations in which the entire chest is to be evaluated. A role for low-dose high-resolution sequential CT remains with the evaluation of the pulmonary parenchyma in cases of suspected diffuse lung disease (García-Peña et al. 2011).

This technique allows scanning at spaced intervals and thus significantly reduces radiation to the patient, while providing excellent spatial and contrast resolution of the lung parenchyma.

In our institutions, we tend to use the sequential HRCT studies in the follow-up assessment of children with chronic lung disease such as cystic fibrosis and interstitial pneumonia (Ambrosino et al. 1994; Lucaya et al. 2000b; García-Peña and Lucaya 2004).

Several techniques are used for data acquisition in helical studies of the chest: standard helical CT, high-resolution helical CT, dynamic helical CT, and low-dose helical CT.

With newer MDCT scanners with multiple detector banks (64 slice +) the narrow collimation (0.6 mm) allows for a study to be performed, of high enough contrast and spatial resolution to allow optimal imaging for both mediastinal and lung parenchymal anatomy without the dose penalty that is incurred with older MDCT scanners.

The modern scanner and the dose reduction methods described above have reduced the dose of this protocol, to such a level that the value in terms of high quality parenchymal and mediastinal imaging in a single study, far outweighs the negligible increase in dose compared to the thicker collimated studies previously performed. We term this a “combiscan.”

This protocol (Table 1) has largely replaced the ‘routine chest protocol’ at our institution for most indications. This study has particular value in the assessment of vascular anomalies, tracheobronchial stenosis, dehiscence, endobronchial lesions, and central airway disease. The thinner collimation allows for excellent Multiplanar and 3D reconstructions. These can be useful in the evaluation of airway abnormalities, certain vascular lesions and cervicothoracic or diaphragmatic and peri-diaphragmatic lesions. 3D images can be rotated to optimally display pathologic entities and selected parts of the reconstruction that can then be analyzed separately.

Helical high-resolution CT scanning of the lung is performed with thin sections (0.5–1 mm) using a high-resolution reconstruction algorithm. This technique is similar to high-resolution CT scanning, but involves continuous data acquisition (Engeler et al. 1994). Lowering the milliamperage setting reduces radiation dose, but the continuous data acquisition of helical CT still delivers more radiation than the low-dose interval high-resolution CT technique (Table 2), in which acquisition is performed with thin collimation and wide sampling intervals.

Dynamic helical CT has enabled scanning at maximum inspiration (TLC, i.e., total lung capacity) and rescanning with an additional spiral acquisition at maximum expiration. This volumetric expiratory method has been used to evaluate lung attenuation in patients with air trapping and emphysema. However, it requires cooperation with breath holding at end expiration, and in young patients <5 years breath holding is problematic.

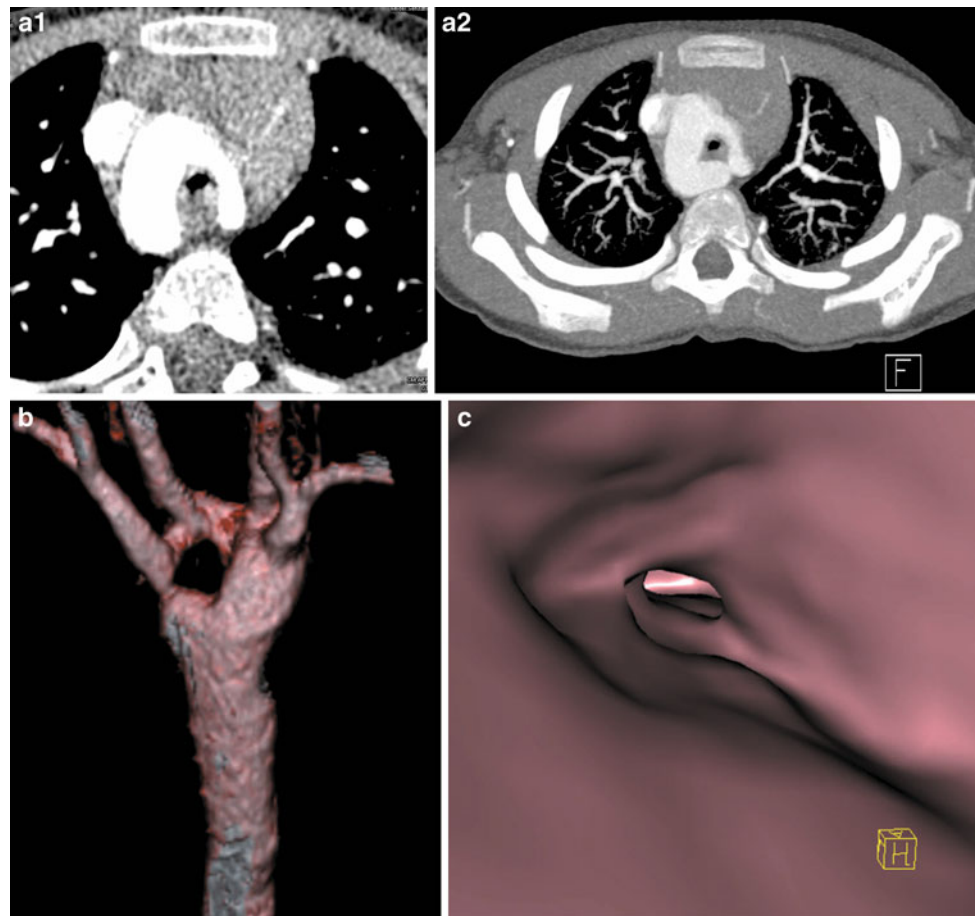
In our practice, we do not use this technique routinely to evaluate air trapping and emphysema.

We prefer three spaced expiratory scans with a low-dose high-resolution technique (Lucaya et al. 2000a). In a non-cooperative child, 2 decubitus slices with the child lying on both sides, i.e., 2 in the right, and 2 in left decubitus positions, shows expiration in the dependent lung (Papaioannou et al. 2007).

Minimum Intensity Projections (MinIP) reconstructions of standard volume acquisitions are also an excellent method for the evaluation of heterogeneous lung parenchymal attenuation where the hyperlucent lung is a reflection of air trapping.

Software programs (available on some helical scanners) have enabled dynamic CT densitometry of the lungs (Johnson et al. 1998b). Dynamic helical CT can also be used to demonstrate respiratory changes in the cross-sectional area of the central airway, e.g., in patients with tracheobronchomalacia (Lee et al. 2009). Dynamic airway assessment may also be achieved with newer techniques such as cine MDCT and four-dimensional (4D) MDCT (Lee et al. 2010b, 2013).

Fig. 8 Double aortic arch in a 1-month-old boy with important respiratory distress. This illustrates the more common right dominant double aortic arch on CTA: the right arch is larger than the left which is stenotic at the origin of the left subclavian artery. Note the marked narrowing of the airway at this level. **a** Thin axial image (**a₁**) and axial maximal intensity projection (MIP) (**a₂**). **b** Posterior volume rendered tomogram (VRT) image of the aorta showing the double aortic arch encasing the trachea. **c** Virtual bronchoscopic image shows concentric tracheal narrowing related to complete encirclement of the trachea by the double arch



Dynamic CT has been used in adults in the preoperative assessment of tracheomalacia, but the high-radiation dose has previously limited its use in children. However, the advent of 320 slice scanners allows the whole thorax to be scanned in a single tube rotation or less. The effective doses for these studies have been shown to be reduced in comparison to scanners with less coverage (Lee et al. 2009, 2010a; Joosten et al. 2012).

Low-dose helical CT scanning can be used in many situations. The X-ray tube current should be as low as possible, without compromising image quality (Takahashi et al. 1998; Rogalla et al. 1999). With helical CT technique, a further reduction in radiation dose can be achieved by increasing table speed if automated dose modulation is not available or not enabled. Use of a targeted approach to image localized processes can also reduce the radiation dose administered.

The performance of high-quality helical CT requires proper selection of technical parameters, including collimation (section thickness), field of view (FOV), table speed (or pitch), reconstruction intervals, reconstruction algorithms, scan time duration, exposure factors (kilovoltage and milliamperage), and scan initiation (Brink 1995; Frush and Donnelly 1998; Frush et al. 2002). These parameters

should be based on the patient's size and the body part to be examined. However, reduction in some of these parameters can lead to problems. Noise increases with decreasing collimation. Scan coverage decreases with reductions in collimation and table speed. Radiation dose increases with reductions in table speed and with reduction in collimation. Decreasing the reconstruction intervals increases processing time.

So, the final choice of parameters always involves a balance between these options to achieve diagnostic image resolution and a low effective dose to the patient.

MDCT scanners have subsecond gantry rotation times. So, reducing rotation time from 1 to 0.5 s, we will halve the radiation dose and the scan time if the mA is fixed (i.e., ADM is not enabled).

The kVp has not routinely been adjusted historically for body CT exams in children. Reducing the kVp reduces the radiation dose substantially, that is in an exponential fashion. In our experience, when the voltage is dropped from 120 down to 80, the radiation dose is decreased by 40 %.

The effect on image quality is important, as both image noise and tissue contrast are affected. The kVp can be reduced (to 80 or 100), related to the child's size or when scanning body regions with high inherent contrast such as

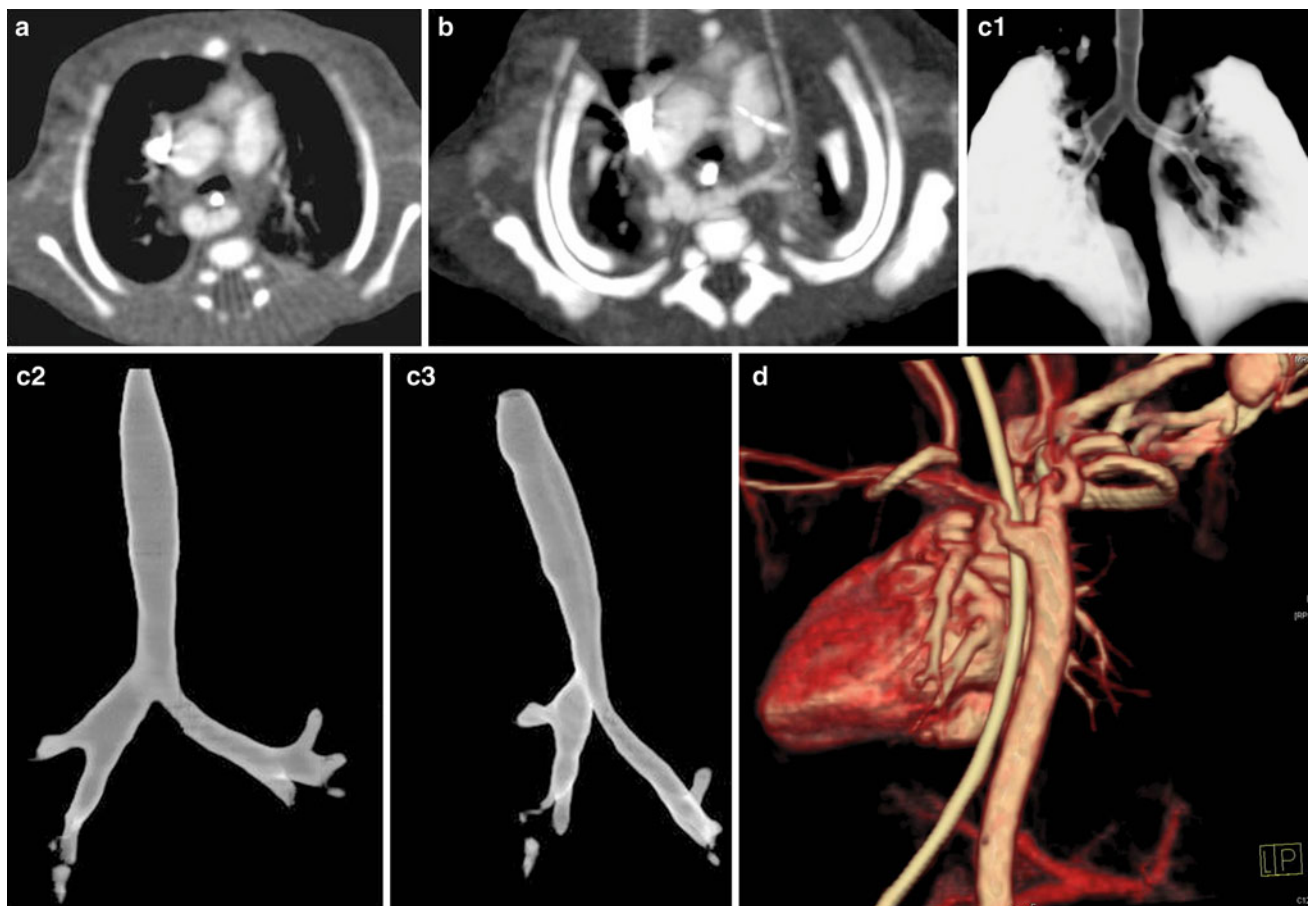


Fig. 9 Kommerell diverticulum with dominant right aortic arch and aberrant left subclavian artery (SCA) arising from the diverticulum in an 8-month-old girl. **a** On axial CT, a vascular structure is seen behind the esophagus. **b** Axial MIP image depicts a right aortic arch, the diverticulum, and left subclavian artery behind the esophagus. **c1, c2, c3** VR

bronchogram demonstrate the tracheobronchial tree, with narrowing of the trachea and left main bronchus. A round structure should be always checked in different planes (coronal, sagittal, and oblique). **d** Posterior oblique VRT image of the mediastinum better shows the right aortic arch and Kommerell diverticulum with left subclavian artery

the chest, airways, and in skeletal studies and CT angiography (Heyer et al. 2007).

The number of detector rows can also affect effective dose via radiation exposure. MDCT scanners have an inherent dose problem in relation to the X-ray beam, which extends beyond the confines of the detector rows (over-scanning). This effect decreases with more detector rows.

In modern scanners, the X-ray beam is filtered, contouring its shape very closely to remove photons that otherwise will be absorbed by the patient, thus decreasing the radiation dose to the patient.

This process is known as z-axis collimation and is most effective over short scan distances and with greater pitch. This is obviously of particular relevance in pediatrics (Christner et al. 2010).

Post-processing techniques using noise reduction filters can allow the use of low mAs (lowering effective dose) and thus improve the quality of the images for diagnostic purposes (Kalra et al. 2003).

Nowadays, most of the MDCT scanner manufacturers make efforts to help with radiation dose control. They have made changes in their equipment to give information on dose and on how to use modulation dose systems to maintain image quality. They have produced age and (much more appropriately) size/diameter adjusted protocols, which are useful as a guide for pediatric dose reduction.

The image reconstruction interval is usually set at an interval equal to the collimation. If multiplanar or 3D reconstructions are required, reconstruction with 50 % overlap can be performed for better definition. Moreover, overlapping images increase lesion depiction, which is useful in the evaluation of small pulmonary nodules.

The raw volumetric data is currently reconstructed using an algorithm based on filtered back projection. This algorithm is not able to consistently produce diagnostic quality images with low mAs (i.e., low-dose examinations) as the background noise produced is excessive. The more recent algorithm for noise reduction in low dose studies has been

discussed above, i.e., adaptive statistical iterative reconstruction (ASIR).

ASIR uses a series of statistical models to reduce image noise and produce studies with dose savings in excess of 30 % (Silva et al. 2010; Yanagawa et al. 2010).

The most frequent reconstruction algorithm used is the low-spatial frequency (standard) algorithm. As routine in our institution, the pulmonary parenchyma is analyzed with a high-spatial frequency algorithm (bone algorithm).

Scan duration should be tailored as much as possible to the breath-holding ability of the child. The scan delay time varies with the region of interest and the clinical indication of the study (Table 1). The scan delay time for CT angiography (Table 3) is more complex and will be the arterial time, obtained by monitoring the contrast enhancement in the descending aorta. This is done by acquiring very low mA scans at the same level (one scan every 3 s over 15 s) and determining the time of peak contrast when the spiral data acquisition should be commenced.

Alternatively, an automated bolus-tracking technique can be used to monitor contrast enhancement and initiate scanning. Scanning begins once an arbitrary threshold level of contrast enhancement is reached within a predefined region of interest (ROI chosen as 100 HU in our institutions). There are limitations with this technique if the scanner protocol is not adjusted for the relatively high heart rates of children. This can result in optimal contrast enhancement being missed due to erroneous (delayed) scan initiation.

Specific recommendations for the selection of parameters are given in the examination protocols presented above (Tables 1, 2, and 3).

2.10 Image Postprocessing

Standard post-processing techniques include four reconstruction displays: Multiplanar Reformats or reconstructions (MPRs), 3D Shaded-Surface-Displays (SSDs), Multiprojective Volume Reconstructions (MPVRs), and 3D Volume Renderings (VRs) (Fig. 1).

The axial images include all the information about the anatomy that is provided with 2D and 3D reformats and it is this information that should be used for most diagnostic purposes. However, postprocessing gives added value to imaging when analyzing oblique structures as well as interfaces and surfaces parallel to the axial plane which are poorly demonstrated and sometimes occult on standard views. 2D and 3D reconstructions are also useful for display of pertinent findings to clinicians and for preoperative planning.

Multiplanar Reformations (MPRs) (Fig. 1a) provide additional diagnostic information in different planes and are as accurate as the axial scans because the data is acquired isovolumetrically. MPRs are 1-voxel-thick, 2D tomographic

sections that can be displayed in standard coronal and sagittal planes, but can in fact be reconstructed in any plane required or in a single tomographic “curved” plane, along the axis of a structure of interest, e.g., a bronchus or a feeding vessel (Salvolini et al. 2000; Siegel 2003). They are real-time, easy-to-reconstruct images, producible as soon as the axial sections are completed. They generally improve our perception of images and give information that although contained in transverse images, is less effectively displayed. Their diagnostic value is substantial in demonstrating and documenting the presence of small focal lesions, defining the vertical extent of a bronchial stenosis, which may go undiagnosed from the axial source CT images, and are invaluable prior to surgical remodeling of vascular rings and the tracheobronchial tree. However, to avoid misinterpretations due to partial volume effect, e.g., overestimation of the degree of a stenosis, overlapping and thinner cuts should be applied when processing the raw data. Likewise, when processing curved MPRs, the trace should be centered within the lumen of interest to avoid anatomic distortion.

Three-dimensional (3D) imaging is a diagnostic tool necessary only in certain cases as it usually requires more time and post-processing skills to provide information already included and demonstrated in the axial images and the MPRs. There is no doubt however that the 3D reformatted images may further increase the diagnostic confidence.

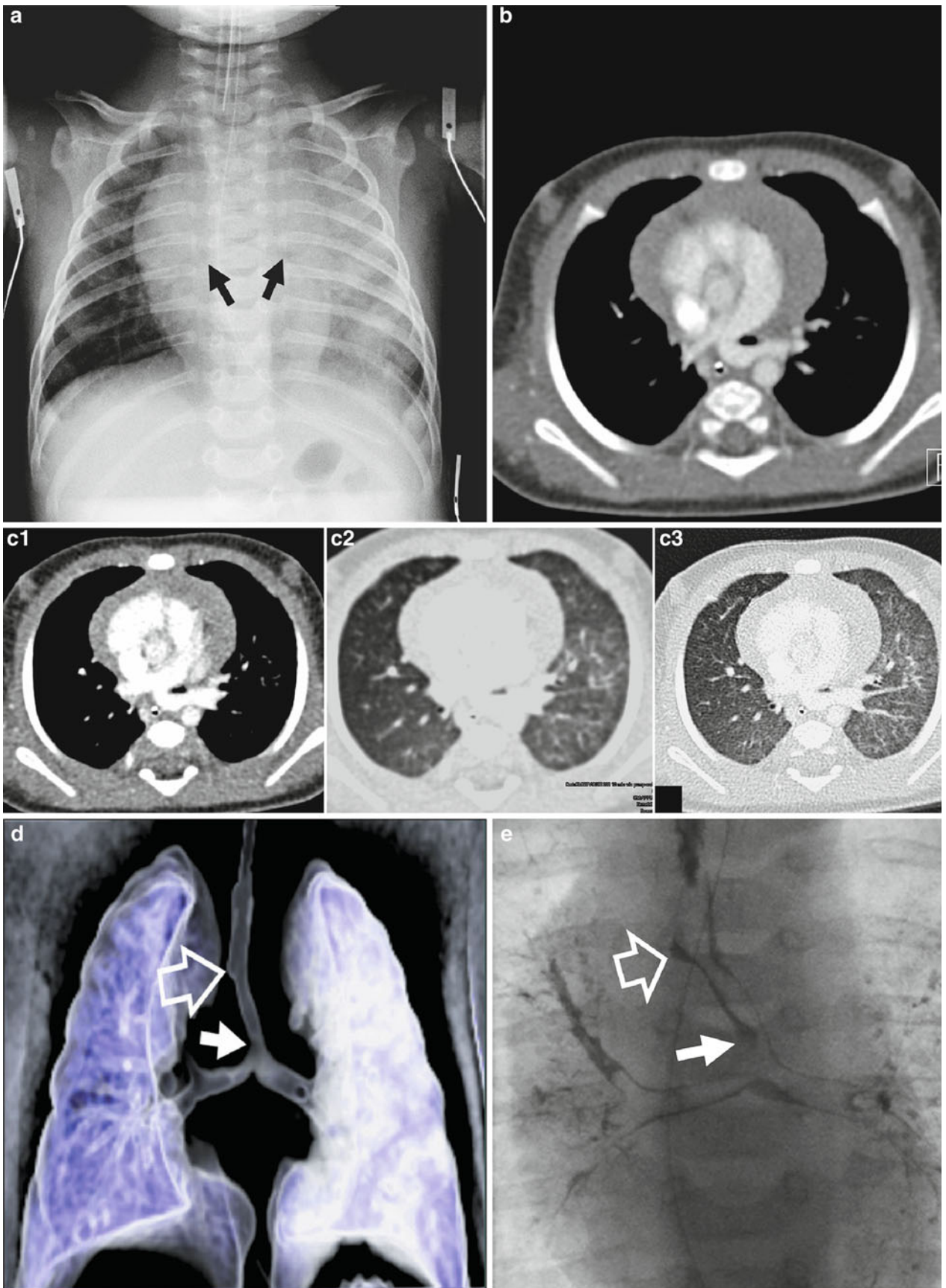
Shaded-Surface-Display 3D Techniques (SSDs) (Figs. 1c, 2c) are applied in the imaging of the central airways, vessels, and bone structures and they are usually more visually impressive than clinically useful.

SSD generates images with depth and 3D information. Using binary classification, voxels with attenuation values above a preset threshold are set to white and voxels with lower attenuation values are set to black (Brink 1995). This method first computes a mathematical model of a surface that connects neighboring pixels with CT intensities above a preset threshold.

Depth or 3D perception is created by shading techniques using an imaginary light source that can be arbitrarily positioned. Such data can be then rotated, allowing the image to be viewed from any perspective.

Their generation from original data is time-consuming and they carry the risk of loss of density information due to problems with thresholding. The threshold must be carefully chosen and should be based on the intensity of the contrast material in the area of interest. The choice of threshold will strongly affect the evaluation of some lesions, such as the degree of stenosis. Choosing too low a threshold may increase noise and also allow the higher density soft tissue to obscure the target vasculature. Choosing a too high threshold may result in small vessels disappearing and/or stenoses being falsely implied.

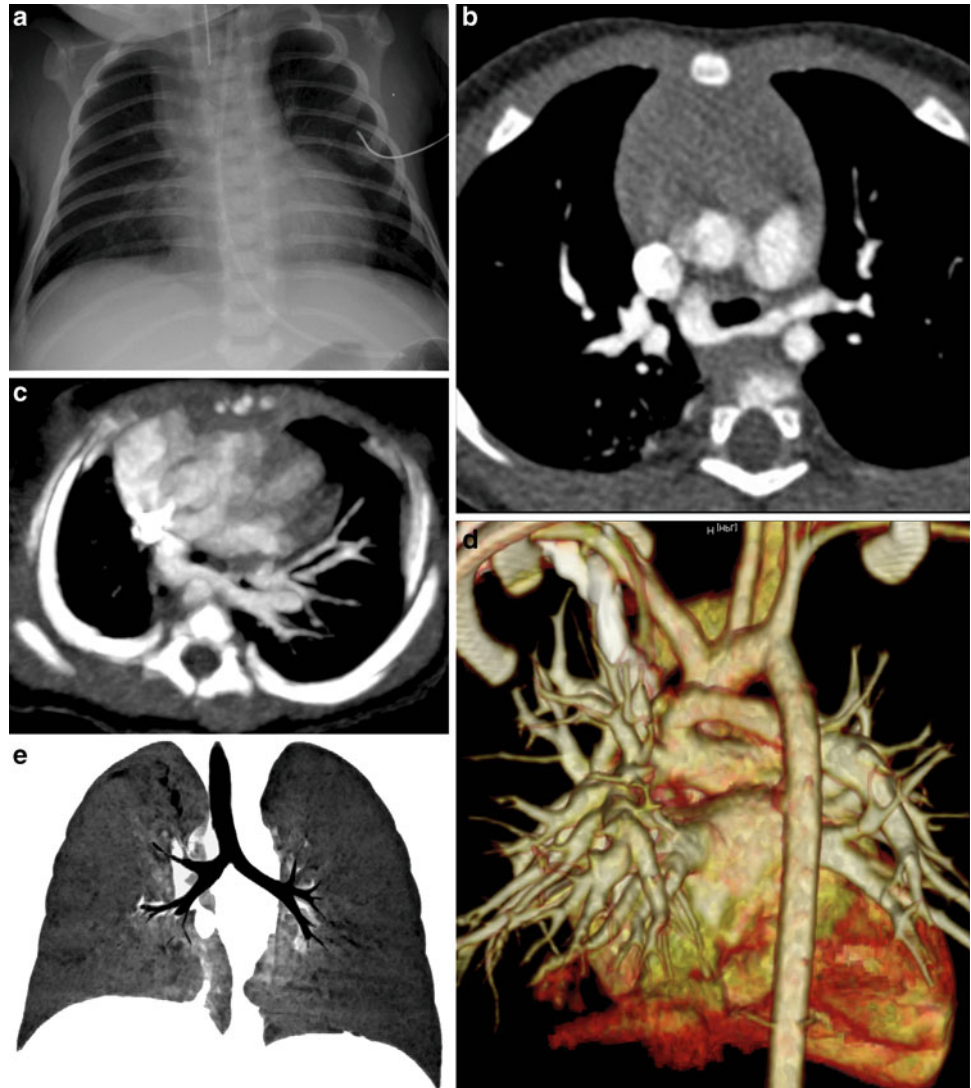
Another problem encountered with SSD is that the reduction of CT volume data to a single surface removes the



◀ **Fig. 10** Pulmonary artery sling. **a** CXR shows widening of the carinal angle due to associated long segment tracheal stenosis and left lung atelectasis. **b** Axial image CTA demonstrates the left pulmonary artery arising from the right pulmonary artery, running between the oesophagus and trachea, which is narrowed. The tracheal narrowing is in fact due predominantly to intrinsic long segment (complete

cartilaginous ring) tracheal stenosis. **c** Axial images showing various post processing algorithms on which the data can be viewed at B30f for soft tissue (**c₁**) and lung parenchyma (**c₂**), and at B60f for high resolution lung parenchymal detail (**c₃**). **d** VR image ‘virtual bronchogram’ shows long segment tracheal narrowing and stenosis alongside. **e** The conventional invasive tracheobronchogram

Fig. 11 Pulmonary sling in a 2-year-old boy with stridor. **a** Chest X-ray with tracheal tube looks normal. **b** On enhanced axial CT and MIP image **c**, the left pulmonary artery is seen to cross the mediastinum between the trachea and esophagus. **d** VR image demonstrates a pulmonary sling, in which the left pulmonary artery arises from the right pulmonary artery. **e** In the MinIP image, there is narrowing of the right bronchus due to vascular compression



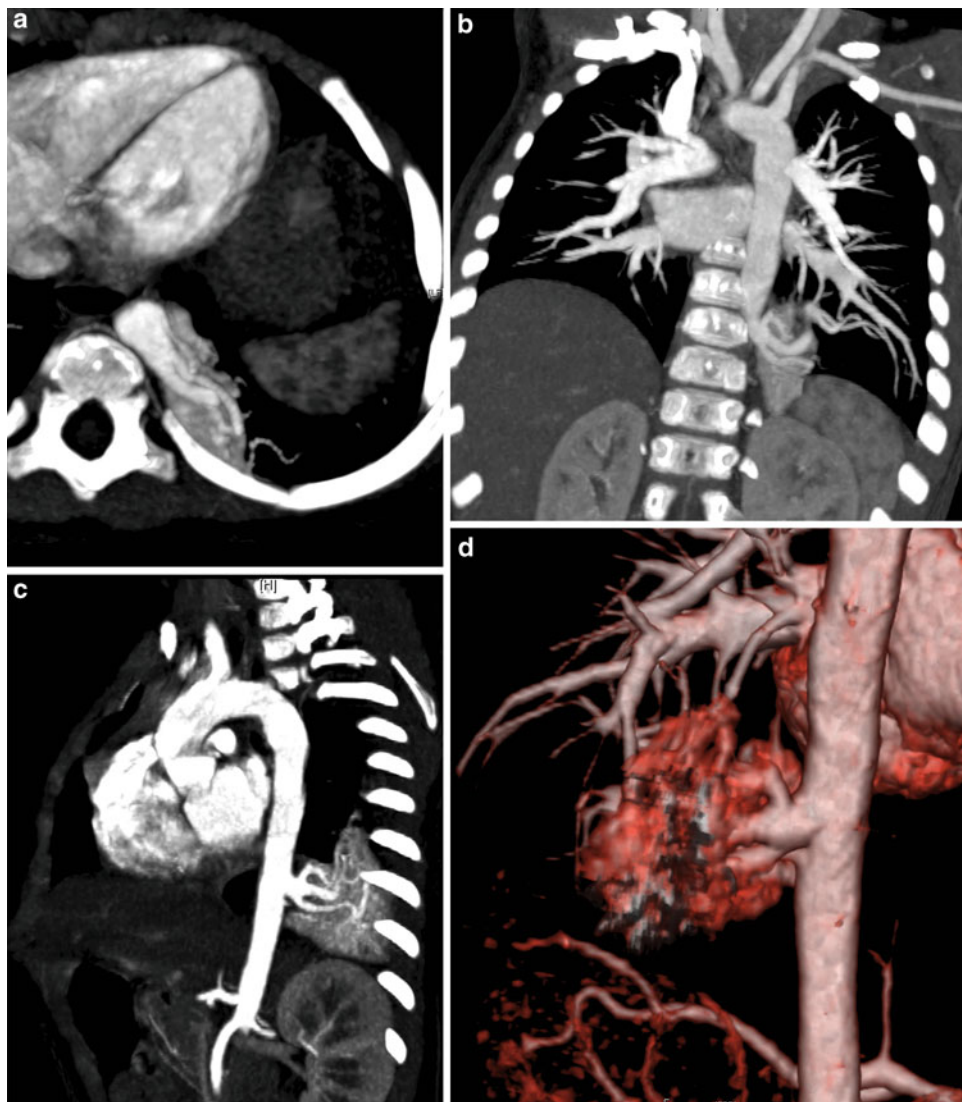
inherent CT quantitative density values, losing gray-scale levels. With this threshold technique one cannot differentiate between solid organ intraparenchymal vasculature and enhancing parenchyma, or between high attenuation structures in vessel walls and intraluminal contrast enhancement.

Multiplanar Volume Reconstructions (MPVR) (Fig. 1b) allow a combination of the spatial resolution of thin sections with the anatomical display of thicker slices and all the information acquired in the raw data set is used. The routine CT images are combined in multiples to create an image thicker in voxels, the volume “slab”, which constitutes

an interactive sum of axial, coronal, and sagittal reconstructed sections (Siegel 2003; Salvolini et al. 2000). By using different algorithms and setting thresholds, maximum (MIP) or minimum intensity (MiniP) voxels can be highlighted within the slab (STS-MIP, STS-MinIP). The sections are typically thin 2–3 mm sections rendered into approximately 20–30 mm slabs (Napel and Jeffrey 1993).

Maximum Intensity Projections (MIP, STS-MIP) Images are generated by mapping the maximum attenuation value along each ray to produce a gray-scale image. Thus, bone and calcified structures are bright and are

Fig. 12 Intralobar pulmonary sequestration in a 1-year-old boy. **a** Axial MIP image shows a solid left lower lobe lesion with possibly two systemic vessels arising from the aorta. **b** Coronal and **c** sagittal MIP images clearly depict a single systemic vessel arising from the aorta and diving into three branches to feed the sequestration. **d** VR image better shows 3D depth perception of the vessel and venous drainage to the left inferior pulmonary vein



distinguishable from both iodinated contrast material and soft tissue. In a vascular examination, it will be necessary to postprocess the image to avoid bone images (Brink 1995).

MIP images are useful for displaying vascular structures, for CT angiography, and for separate parenchymal nodules from surrounding pulmonary vasculature. They reliably display vessel caliber, metallic stents, and wall calcifications, but provide poor separation of overlapping vessels because 3D relationships are lost (Fig. 2). Vascular anatomy is frequently difficult to comprehend from standard cross-sectional images. Blood vessels that are perpendicular or oblique to the section will appear as small circles or ellipses, and may mimic the appearance of a pulmonary nodule. With MIP, one can integrate the path of vessels and their connections with other structures into the larger picture of vascular anatomy (Fig. 3).

The display of MIP images in a cine loop to simulate a rotating viewing direction improves the lack of 3D depth. This allows visualization of 3D relationships and may provide clues to the nature of eccentric stenosis, and the crossing or looping of vessels (Fig. 4).

Minimum Intensity Projections (MinIP, STS-MinIP) Images

MiniP images map the minimal attenuation value to a grayscale image.

MinIP images are valuable in examinations of the central airways (Figs. 5, 6) and in analyzing mild forms of uneven attenuation of the lungs (Remy-Jardin et al. 1993).

MinIPs enable airway anatomy to be visualized and are also useful for displaying the whole volume of parenchymal cysts, bullae, or over inflation. They are also very valuable

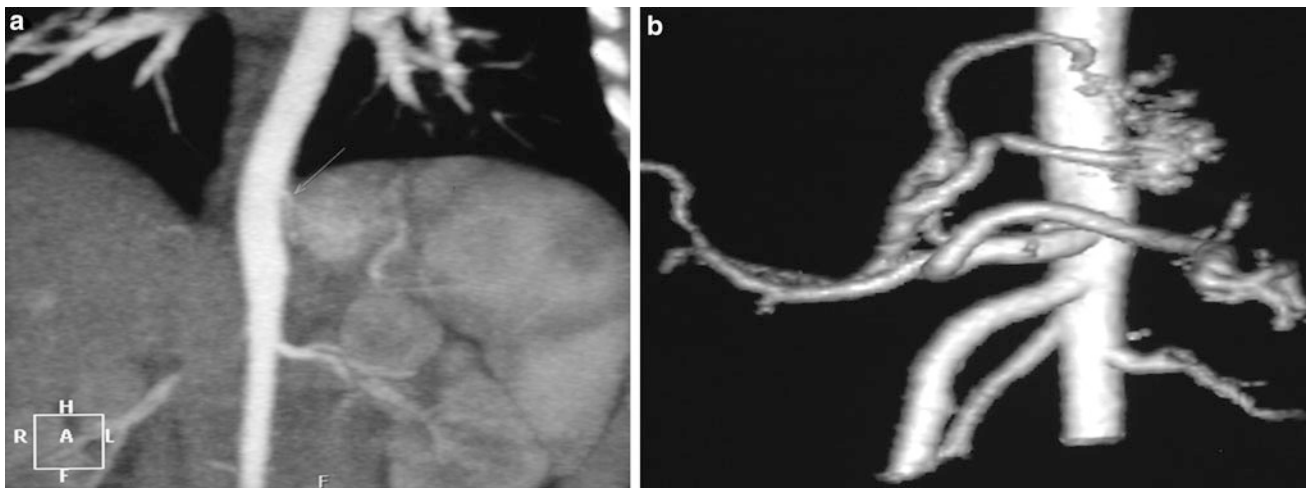


Fig. 13 Extralobar pulmonary sequestration. Prenatal diagnosis of congenital pulmonary malformation. Postnatal CXR was normal. **a** Coronal MIP image shows an enhanced left mass in a subdiaphragmatic

location, and a small systemic vessel arising from the aorta and feeding the mass. **b** VRT demonstrates another systemic vessel from the celiac trunk feeding the mass, and venous drainage to the portal vein

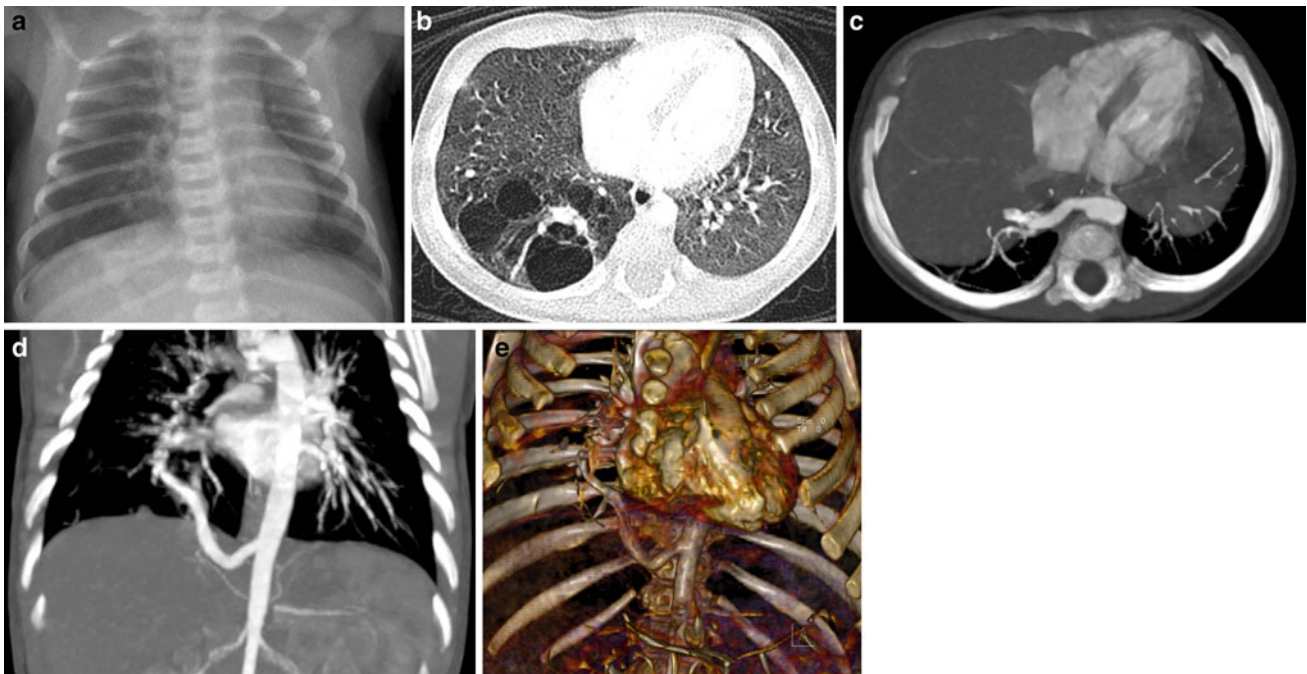


Fig. 14 Congenital pulmonary airway malformation (CPAM) with a systemic vessel in a 6-month-old girl. Prenatal diagnosis of pulmonary malformation. **a** Chest X-ray looks nearly normal, with some linear images superimposed on the liver silhouette. **b** On axial CT of the lungs, multiple cystic areas are seen in the right lower lobe. **c** Axial

MIP demonstrates a systemic vessel arising from the aorta and feeding the right lung base. **d** Coronal MIP image depicts a prominent systemic vessel from the aorta, and a drainage vein to the right inferior pulmonary vein. **e** VR shows similar findings

for delineation of the branching pattern of the tracheo-bronchial tree and the presence of lung isomerism, tracheal bronchi, and airway narrowing.

Visualization of the heterogeneous attenuation of the lung parenchyma as a result of constrictive obliterative bronchiolitis is well portrayed in the coronal plane particularly (Fig. 7).

Volume Rendered Tomography (VRT)

Three-dimensional (3D) volume renderings (VRs) represent the main technique for 3D reformatting of the airways and the vascular structures of the mediastinum.

The VR technique is particularly useful for displaying structures that course parallel or oblique to the transverse

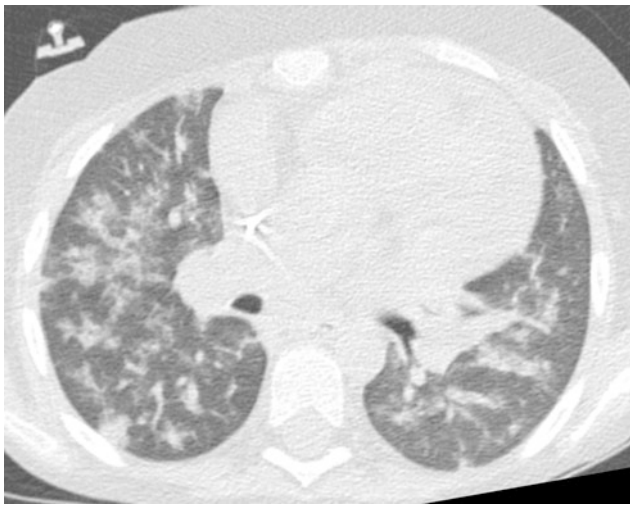


Fig. 15 Bronchiolitis obliterans with organizing pneumonia (BOOP) in an immunocompromised patient. A 10-year-old boy who underwent renal transplantation 1 year previously with mild respiratory distress. On axial CT, there are multiple poorly-defined nodules and areas of ground glass. The lesions disappeared with steroid therapy

plane and those that develop or extend into multiple planes (Salvolini et al. 2000; Siegel 2003) (Figs. 1, 8, 9, 10, 11). Thus the added value in cardiothoracic imaging to depict complex anatomy of the heart, great vessels, and lungs in 3D has revolutionized cardiothoracic imaging (Figs. 12, 13, 14). However, preliminary editing is still necessary and can be time-consuming, altering work patterns in CT.

In VRT, different anatomical tissues are represented by proportional values that are assigned to every voxel and depend on the range of tissue attenuation values in the original data set. Voxels are selected by the probability of belonging to the object of interest; thus they are displayed in different colors or several shades of gray, different transparency, or opacity. Transition from the reconstructed surface to the surrounding media is gradual and the depiction of interfaces, like the inner tracheal lining, is supposed to approach the true appearances.

VRT from extraluminal visualization of the tracheobronchial tree creates images similar to conventional bronchograms and is applicable in clinical practice without the concomitant administration of a contrast agent (Figs. 5d, 6f, 9c, 10d). Other clinical applications include cardiovascular imaging and chest wall disease (Johnson et al. 1998a).

Albeit this 3D segmentation technique is better and more complicated than the others previously mentioned, some information is still lost during processing so that the axial images are still indispensable for the radiologist to assess extraluminal disease and identify artifacts. Three-dimensional VRT reconstructed images are attractive and appealing to the clinicians as they may better illustrate short

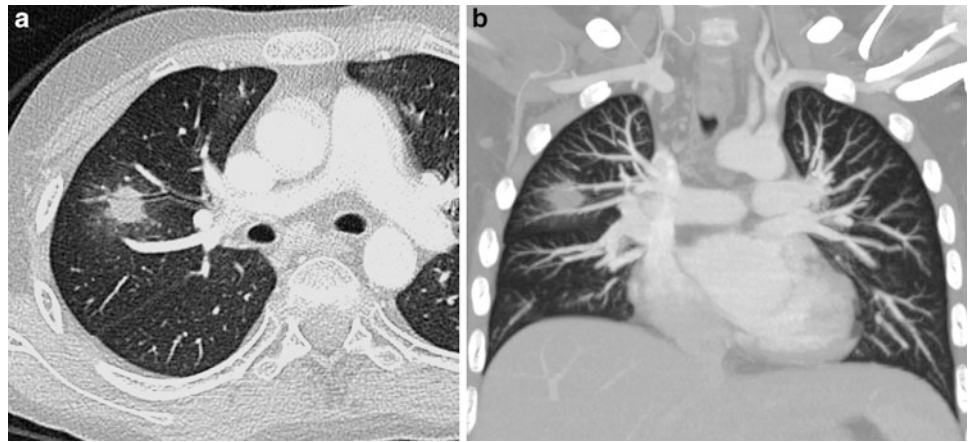
focal areas of narrowing, the craniocaudal length of a tracheobronchial stenosis, and complex congenital cardiovascular and tracheobronchial anomalies.

The inner surface of air-containing tracheobronchial tree can be displayed with Virtual Bronchoscopy (VB) (Figs. 1d, 8c) which is performed with either polygonal SSD or direct VR. VB is a noninvasive and accurate technique that can provide “bronchoscopic” views of the central and the peripheral airways.

This technique is considered supplementary both to CT and the gold-standard of flexible bronchoscopy. Referral to the axial sections is again valuable to recognize artifacts and to gain perception of the orientation within the virtual airways. VB uses perspective surface rendering, which takes advantage of the natural contrast between the airway and the surrounding tissues (Heyer et al. 2004). The point for viewing is located intraluminally so that external structures do not overlap and editing takes shorter time periods. Submillimeter (0.625 mm, 0.75 mm) slice thickness allows deeper penetration and visualization of the bronchial surface down to the bronchial diameters of below 5 mm (Khan et al. 2004; Heyer et al. 2004; Venkatraman et al. 2006). In practice, VB is of limited value, reserved for cases where bronchoscopy is not applicable (children at risk of undergoing traditional bronchoscopy) or precise navigation is not possible to guide airway interventional procedures and in emergencies such as infant airway (tracheal) stenosis that cannot be evaluated otherwise (Khan et al. 2004). The produced images resemble the true bronchoscopic images and can additionally “advance” distally to an airway obstruction, where the real endoscope cannot penetrate (Salvolini et al. 2000; Hoppe et al. 2004). However, when compared to fiberoptic bronchoscopy, VB precludes any therapeutic maneuvering, it is incapable of detecting endoluminal lesions smaller than 2–3 mm, and provides limited information about mucosal details (morphology, vascularity, and color) making differentiation between pathologic processes and retained secretions difficult (Heyer et al. 2004). There is consensus that measurements should be better performed in 2D sections as they may be otherwise inaccurate. The technique is additionally affected by the partial volume effect, which may lead to misinterpretation of severe stenoses as occlusions, and the threshold level is therefore of importance for displaying accurate simulations (Hoppe et al. 2004).

Dynamic and functional inspiratory and expiratory scanning with single breath-hold MDCT helps identification of strictures, areas of air-trapping and tracheobronchomalacia, but is rarely applied in pediatric practice because of the associated radiation burden (Johnson et al. 1998b; Siegel 2003). The advent of the newer dose reduction techniques and more detector rows per scanner make the use of dynamic scanning possible.

Fig. 16 Pulmonary nodules. Post-BMT fungal lesion (*Aspergillus* infection). A 7-year-old boy with BMT due to leukemia. Chest X-ray was normal. **a** Axial CT shows a small nodule in the right upper pulmonary lobe, surrounded by a halo of ground glass. **b** Coronal MIP image better depicts the relationship of the nodule with the minor fissure, and confirms no other nodules



2.11 Newer Advances in CT

Newer developments in Computed Tomography leads to improve their applications within pediatric thoracic imaging.

In essence two basic CT scanner configurations exist:

1. Multidetector CT (MDCT) with up to 320 detector rows
2. Dual-Source CT (DSCT) utilizing MDCT technology.

Advantages of the newer scanners on the market include subsecond tube rotation time (down to 0.33 s), and this increased acquisition speed has the potential to reduce motion and respiratory artifact (particularly problematic in children) and also to improve image quality. The availability of even smaller detector elements (0.5 mm) combined with thin-slice collimation, provides isotropic resolution with accurate reformatted images in any orthogonal plane, and displayed as either 2 or 3D images, that have the same spatial resolution as the base axial data set and with reduced partial volume artifact.

320-Slice MDCT

The advent of 320 MDCT allows larger volume scanning coverage of up to 16 cms. This is manifest as coverage within and above the clinical range of thoracic imaging in neonates and young children. This allows imaging of the entire chest in a single volume cone-beam acquisition, during one tube rotation of 0.35 s (Kroft et al. 2010). This acquisition time is much faster when compared with either helical MDCT or DSCT acquisition. The acquired axial volumetric datasets allow potential for radiation dose reduction related to the large nominal beam width used, so that the contribution of the penumbra effect is less of a problem as it is less prominent.

In addition unlike helical scanning, over-ranging in the longitudinal axis does not apply, as the exposed range

corresponds exactly to the imaged range and so there is more effective use of the radiation exposure for image formation.

Axial volumetric acquisition can be well suited to other clinical situations, such as cardiac imaging in children, where using prospective ECG-gating the entire heart can be imaged in a single tube rotation.

Dual-Source CT (DSCT)

Now in its second generation, the DSCT (Siemens Flash, Forchheim, Germany) is currently the latest in CT technology, incorporating two X-ray tubes and corresponding 64-row detector systems (each contributing 128 slices by means of a z flying focal spot) mounted at an angular offset of 90° relative to one another. Primarily designed for cardiac imaging, the two tube-detector system operates in tandem and not simultaneously. Data from the second detector system is collected a quarter of a rotation later following the first set of detectors, thus allowing gapless volume high-pitch scanning (up to 3.2 pitch), avoiding overlapping slices, and with significant reduction in radiation dose.

This enables a 75 ms temporal resolution, which together with a fast gantry rotation time of 0.28 s, allows helical prospective ECG-triggered cardiac imaging.

The result is that imaging children with high heart rates is no longer a limiting factor, and this is invaluable in both pre- and postsurgical assessment of a wide variety of congenital heart diseases and diseases affecting the pulmonary vasculature.

Improved visualization of the coronary arteries can also be achieved even when data is captured during the less favorable, i.e., systolic phase of cardiac motion (Ben Saad et al. 2009) even in younger children.

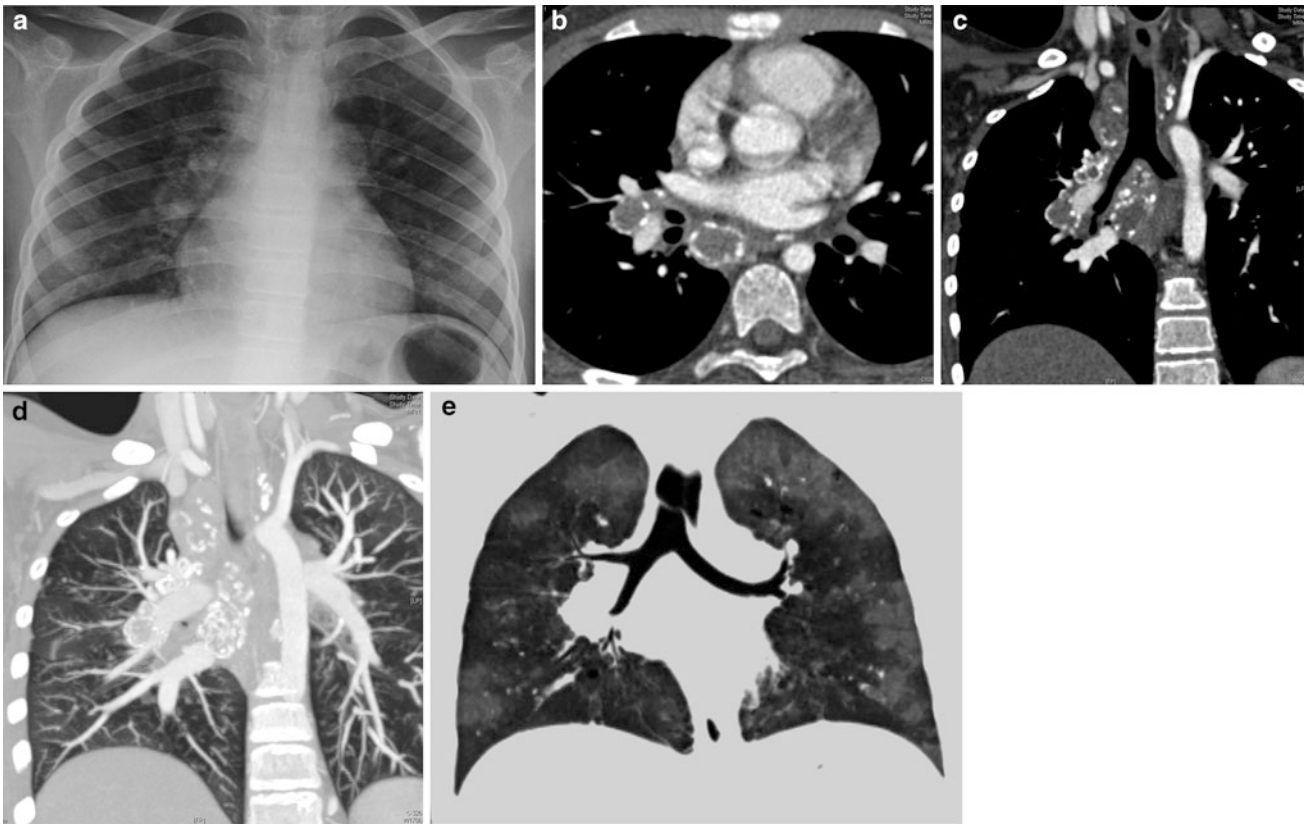


Fig. 17 Mediastinal and hilar lymph nodes in multidrug-resistant TB. A 6-year-old boy with several weeks of fever. **a** Chest X-ray demonstrates multiple masses in the mediastinum and pulmonary hila, with calcifications **b** Enhanced axial CT shows multiple ring-calcified lymph nodes in the right hilum and below the carina,

differentiating masses from vessels. **c** Coronal MPR additionally depicts the extension of the calcified lesions to the right paratracheal space and the left mediastinum. **d** MIP better depicts the relationship between the lymph nodes and the vessels. **e** MinIP image demonstrates bronchial airway compression, and heterogeneous lung attenuation

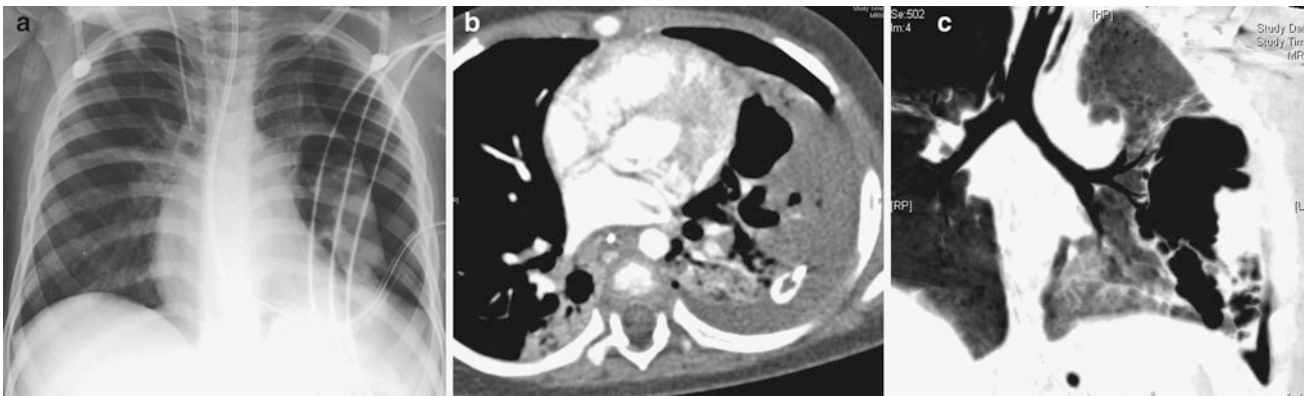


Fig. 18 Bronchopulmonary fistula in pulmonary infection. A 7-year-old boy with fever of several days duration and respiratory distress. **a** Chest X-ray shows a left lung consolidation with pneumothorax. **b** Enhanced axial CT demonstrates considerable left lung

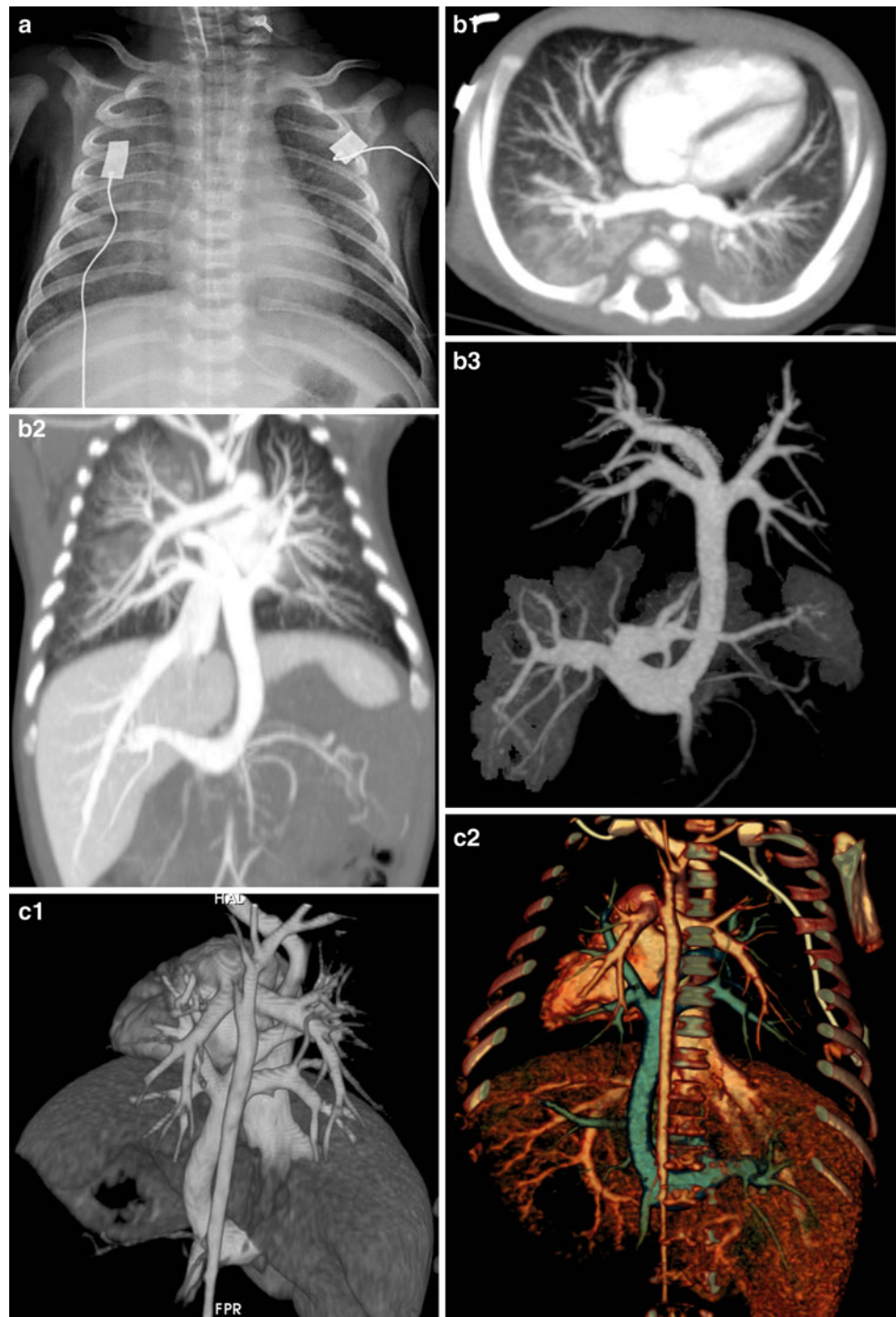
hypoperfusion with necrotic areas, pleural fluid (pleural tube), and a pneumothorax. There is also a small right lung consolidation. **c** Coronal MinIP image better depicts a bronchopulmonary fistula, multiple necrotic air lesions, and a pneumothorax

Dual-Energy Dual-Source CT

The availability of two X-ray tubes allows simultaneous acquisition of two data sets at different tube potentials (80 and 140 kVp) during the same phase of contrast

enhancement. This will exclude both temporal changes and spatial misregistration. The dual energy technique takes advantage of differences between material and tissue composition, and in differences of their photon absorption

Fig. 19 Total anomalous pulmonary venous return to IVC. Newborn with severe respiratory distress. **a** Chest X-ray shows increased density in both lungs due to pulmonary edema, with no cardiomegaly. **b1**, **b2**, **b3** MIP images and **c1**, **c2** VR images disclose that the pulmonary veins do not enter the left atrium. The four pulmonary veins joint to a collector that drains into the portal vein. Hepatic veins are also prominent



characteristics. In particular, material with high atomic numbers (like iodine) will exhibit a different degree of attenuation between the two different tube potentials.

By applying a specific post-processing algorithm to the acquired data, virtual unenhanced and virtual angiographic data sets can be generated based on the three-material

composition principle, i.e., within the chest, soft tissue, air, and iodine are analyzed. By application of a bone removal algorithm, an angiographic dataset without overlying bony structures for easy interpretation can be viewed. Overall radiation dose associated with dual-energy CT (DECT) is noted to be comparable to that of single source MDCT system.

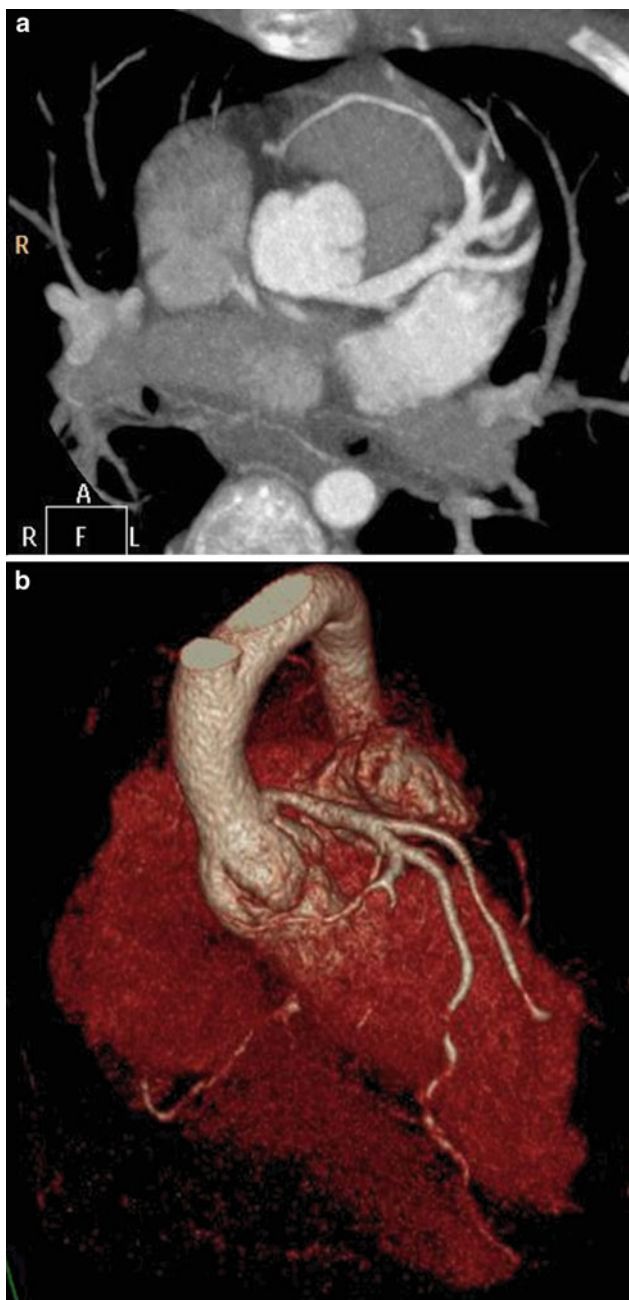


Fig. 20 Congenital coronary anomalies. Single coronary artery in a 6-year-old boy. Coronary MDCT angiography. **a** Axial MIP image shows a single prominent left coronary artery. There is no ostium for the right coronary artery. **b** VR image displays the left coronary artery and one of its branches supplying the apex and right ventricle

Other clinical dual-energy application includes characterization of abdominal masses, chemical composition of renal calculi, myocardial and pulmonary perfusion imaging.

Within thoracic CT an important area for dual energy imaging is in the depiction of iodine distribution for the detection of peripheral lung perfusion defects, which result from pulmonary emboli. This application adds important

additional functional information to conventional structural pulmonary CT angiography and has an application in the evaluation of subsegmental pulmonary emboli (Johnson et al. 2007; Hoey et al. 2009).

When advanced post-processing software is applied to the acquired data set, an iodine distribution map is generated and overlaid onto a gray-scale image. Normal perfusion images show homogeneous color distribution extending to the lung periphery and when displayed in a multiplanar format can be manipulated manually.

The presence of a filling defect or hypoperfusion of lung parenchyma will indicate an obstructed pulmonary vessel supplying the relevant lung segment. Review of the gray-scale image will help to determine the anatomical site.

Xenon Ventilation in Chest Imaging

Another potential for the use of DECT is its application with the use of xenon ventilation in thoracic imaging. This technique has been described as more sensitive in the evaluation of both regional and global airway/lung abnormalities in children (Goo et al. 2010).

Conventional CT requires both inspiratory and expiratory acquisitions in order to demonstrate air trapping within the lung parenchyma.

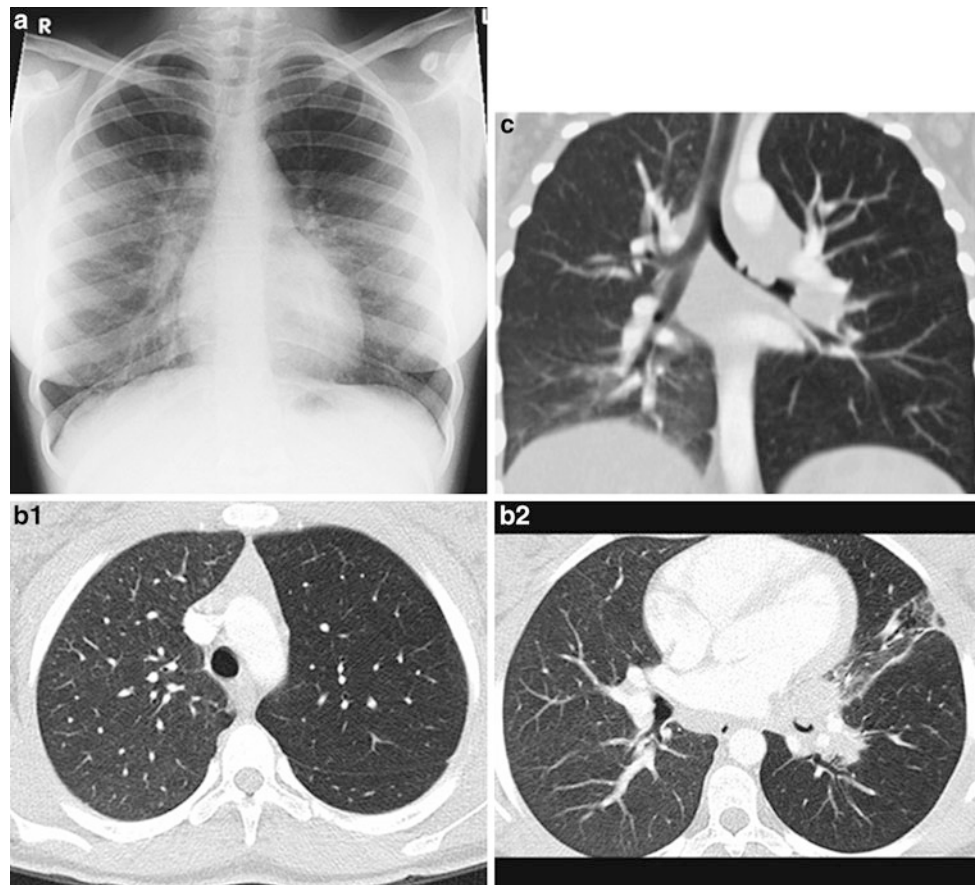
Xenon ventilation, which demonstrates regional ventilation defects on inspiration will obviate the need for an additional expiratory phase acquisition and hence show a reduction in radiation dose.

Also problematic in children is the quantitative evaluation of lung density on CT, which is highly age dependent, and varies with the level of cooperation of the patient to breath hold at total lung capacity (TLC). The use of xenon with its insensitivity to degree of lung expansion can provide more accurate assessment.

3 Helical Chest CT Main Applications

The introduction of helical technology has extended the clinical indications of chest CT (García-Peña and Owens 2008). The most important diagnostic indications in children include evaluation of pulmonary nodules and thoracic masses (Agrons et al. 1998; Bal et al. 2004; Paterson 2005; Valencia et al. 2006; Mc Hugh 2008), lesions located in difficult areas (e.g., cervico-thoracic, diaphragmatic, peridiaphragmatic, or chest wall regions) (Ahn et al. 2010) and in the central airways (Berrocal et al. 2004; Yedururi et al. 2008), definition of vascular anatomy, and study of critically ill patients, including trauma patients. In our institution, the most common indications for chest studies are the detection and characterization of pulmonary nodules and definition of mediastinal masses in children with known or suspected malignancies, investigation of infection

Fig. 21 Intrabronchial aspergillus infection with persistent overinflation of the left lung related to delayed diagnosis of bronchopulmonary aspergillosis secondary to chronic granulomatous disease (CGD). **a** CXR relatively unremarkable. **b** Axial CT images (**b₁** and **b₂**). The left main bronchus shows an endoluminal polypoid mass with distal overinflation of the left lung due to ball valve effect. **c** Coronal multiplanar reformation (MPR) image through the left main bronchus show overinflation of the left lung compared to the right and the soft tissue images show endoluminal bronchial wall thickening causing ball valve effect in the left lung



in immunocompetent and immunocompromised child (Fig. 15), congenital malformations, combined airway and vascular studies (Figs. 1, 8, 9, 10, 11), and cardiovascular studies (Harty and Kramer 1998; Lobo and Antunes 2012; Dillman et al. 2011; Garcia-Peña et al. 2013). The diagnosis and follow-up of bronchiectasis and diffuse lung disease can also be carried out by MDCT, but an HRCT technique is preferable, because radiation dose should be low when evaluating chronic disease (Lucaya et al. 2000a; Garcia-Peña and Lucaya 2004; Brody et al. 2004; Lucaya and Decou Le Pointe 2008; Klusmann and Owens 2009; Garcia-Peña et al. 2011).

3.1 Evaluation of Pulmonary Nodules and Chest Masses

Several studies have demonstrated that at least 10 % more pulmonary nodules can be identified with helical than with conventional CT (Costello et al. 1991; Remy-Jardin et al. 1993). The ability to obtain overlapping reconstructions at smaller intervals with the contiguous volume data acquired increases the certainty that scans are obtained through the

center of any lesion. These images depict the lesion without volume-averaging effect.

In patients with suspected metastatic disease, use of helical CT with a single breath-hold technique eliminates respiratory misregistration caused by variations in the depth of respiration. This results in better ability to detect small nodules. In children unable to breath-hold who must be scanned during quiet respiration, helical CT has shown no significant loss of accuracy in the detection of pulmonary metastasis (Coakley et al. 1997a). The problem of variable respiratory excursion is further minimized by volume acquisition and the possibility of overlapping image reconstruction (Buckley et al. 1995; Coakley et al. 1997b).

The volumetric data created during helical CT and the coronal and sagittal images reconstructed from them are useful for delineating the anatomy of vascular lesions that appear similar to nodules. MIP images are extremely useful for differentiating nodules from vessels. Detection of small nodules on MDCT may be improved with the use of MIP and sliding thick slab MIP (Coakley et al. 1998; Valencia et al. 2006; Kawel et al. 2009). Multiplanar image reconstructions can clarify the spatial relationships of a nodule to the pleura or diaphragm (Brink et al. 1994a; Ahn et al.

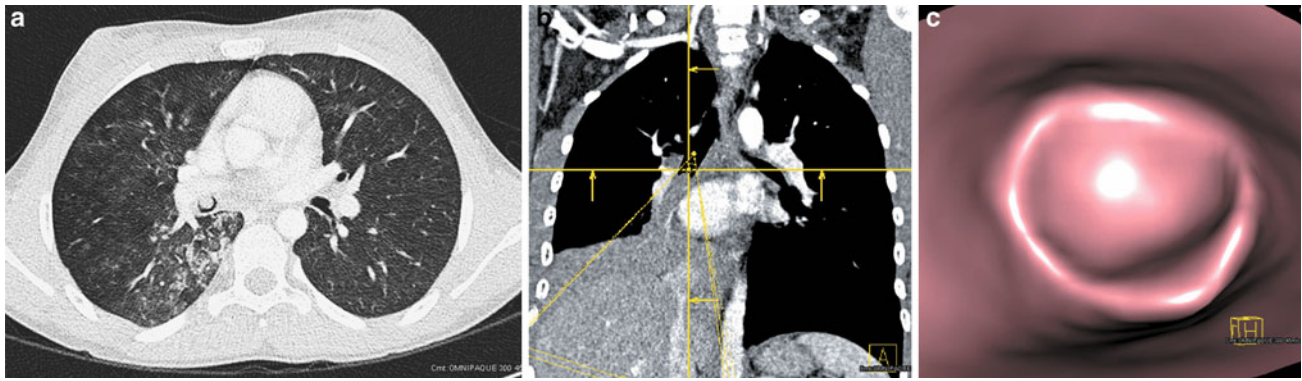


Fig. 22 An HIV infected patient with TB and massive haemoptysis secondary to endo bronchial and cavitary TB shows polypoid obstruction of the R main bronchus seen on the a–c images. **a** Axial CT image. **b** Coronal MPRs with a tubular soft tissue mass in the

RMB. **c** Virtual bronchoscopy (view from the carina) shows the obstructing mass in the RMB. The coronal MPR image indicates the viewpoint

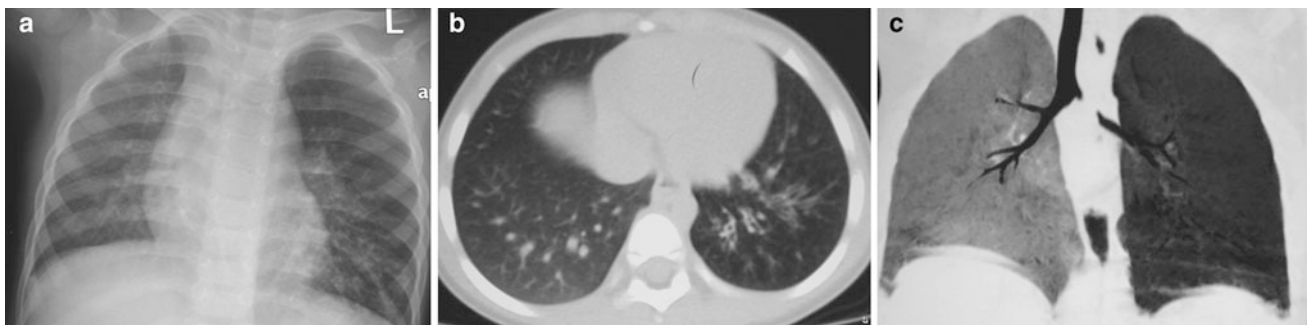


Fig. 23 Intrabronchial hamartoma in the left main bronchus in a 2-year-old boy with repeated pneumonia of the left lung. **a** Chest X-ray shows hyperaeration of the left hemithorax with increased density of

the LLL. **b** Coronal CT depicts the left emphysema and bronchial thickening secondary to repeated infections. **c** MinIP image confirms the obstructive emphysema due to a left bronchial hamartoma



Fig. 24 Intrabronchial mucoepidermoid carcinoma in an 11-year-old boy with repeated left lung atelectasis. **a** Chest X-ray shows increased density of the left pulmonary base, with elevation of the left diaphragm

due to left lung atelectasis. **b** Coronal MPR depicts obstructive emphysema, and a mass within the left bronchus. **c** On virtual bronchoscopy (VB), the mass is seen to occupy the left bronchus

2010), a task that is especially difficult with conventional section-by-section CT because of the large excursion of the diaphragm between breaths. CT detection of small pulmonary nodules usually causes less of a dilemma in children than in adults, but the differentiation between benign and malignant pulmonary nodules can also be difficult (Fig. 16) (Mc Carville et al. 2006).

Low-dose helical CT of the chest is highly sensitive for detecting pulmonary nodules, and could be an ideal alternative to conventional-dose helical CT for screening purposes (Gartenschläger et al. 1998). Recommendations for the selection of parameters are given in the “Routine Chest Protocol” (Table 1). Intravenous contrast agents are not usually needed in the evaluation of pulmonary nodules.

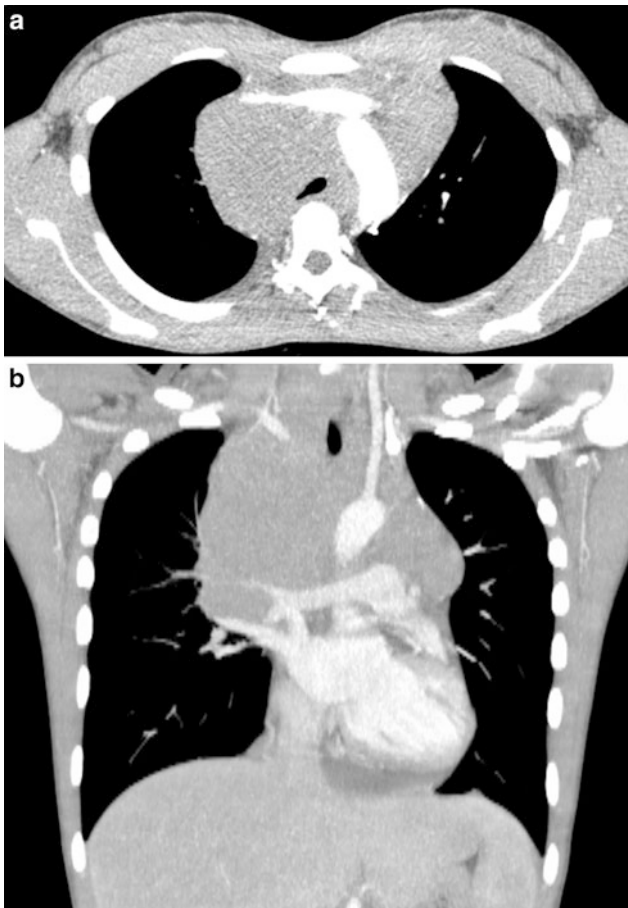


Fig. 25 Lymphoma with mediastinal and cervicothoracic masses in a 10-year-old boy with fatigue and fever. **a** Axial CT shows a bilateral mediastinal mass and considerable tracheal compression. **b** Coronal MIP better demonstrates the cervical extension of the mass and the tracheal compression

To assess solitary pulmonary masses and mediastinal lesions, another indication of helical CT, we recommend the Routine Chest Protocol with IV contrast material (Table 1). The rapid scanning speed facilitates scanning during the time of peak contrast enhancement, permitting optimal definition of anatomic features. This is particularly important in children, who have little fat and lack intrinsic contrast differences.

Scanning during peak contrast levels optimizes the evaluation of mediastinal and hilar lymph nodes and masses. Mediastinal vascular structures and masses are easily differentiated (Fig. 17). Helical CT is an excellent modality for assessing anterior or middle mediastinal masses and possible lung parenchyma involvement, but MRI is increasingly taking its place in evaluating masses. Posterior mediastinal masses can also be studied by helical CT, but MRI is the procedure of choice in these cases, as mostly they are neurogenic tumors. Special attention should be given to intraspinal extension.

CT provides excellent spatial resolution and considerable detail. The pulmonary parenchyma is optimally visualized on CT as opposed to MR imaging (Newman 2011), and calcification is better seen on CT.

Other important indications for helical CT are tumor staging and follow-up evaluation of treatment, and particularly, assessment of lung metastasis. As compared with conventional CT, helical CT can facilitate identification of infiltration, vascular encasement, airway displacement, and enlarged hilar lymph nodes. Multiplanar reconstructions can be very useful for identifying infiltration, encasement, or compression of vital structures, and intraspinal extension. The resulting information facilitates surgical planning and radiation therapy. Another advantage is that chest and abdominal studies can be performed in a single session with a single dose of IV contrast material. This is especially important in the evaluation of patients with lymphoma.

Other abnormalities that are well seen on helical CT studies at peak contrast enhancement include congenital large vessel abnormalities (Trinavarat 2011) (Figs. 8, 9, 10, 11), congenital chest masses (pulmonary sequestration, cystic congenital pulmonary airway malformation) (García-Peña et al. 2013) (Figs. 12, 13, 14), pulmonary and pleural infections (Fig. 18), chest trauma, surgical shunts and postoperative vascular anatomy, vascular masses (angiomas, lung fistula, varix), central pulmonary thromboemboli (Remy-Jardin et al. 1992; Lee et al. 2012), and cardiac and coronary evaluation (Goo et al. 2009; Saad et al. 2009).

3.2 Evaluation of Vascular Anatomy: CT Angiography

CT angiography is relatively new, and possibly one of the most important applications of helical CT (Choo et al. 2006; Lawrence 2008; Marini et al. 2009; Poole and Ferguson 2010; Chung et al. 2010; Khandelwal et al. 2011). CT angiography provides high-quality vascular imaging, and can depict congenital and acquired vascular abnormalities of the chest in children. Standardized CT angiography and arterial timing bolus test (or bolus-tracking technique) protocols are recommended in such cases (Table 3). Optimal contrast enhancement is best achieved using a power injector, which should be used whenever possible. With CT angiography, one can analyze vascular abnormalities of the pulmonary arteries, aortic arch and great vessels (double aortic arch, pulmonary sling, etc.) (Figs. 1, 8, 9, 10, 11) (Katz et al. 1995; Ghersin et al. 2005; Turner et al. 2005), pulmonary vein anomalies (Fig. 19) (Ou et al. 2009; Vyas et al. 2012), cardiac and coronary lesions (Fig. 20) (Saad et al. 2009; Goo et al. 2009; Lapierre et al. 2010; Siripornpitak et al. 2011), cardiac surgery postoperative status (Marini et al. 2009), and vascular lesions (Khandelwal et al.

Fig. 26 Diaphragmatic lesion due to reherniation after congenital diaphragmatic hernia repair. A 1-year-old boy with successful previous repair of a congenital diaphragmatic hernia, again presented an abnormal left diaphragm. **a** Chest X-ray after neonatal surgery shows a normally located left diaphragm. **b** Chest X-ray 1 year later depicts opacification of the left pulmonary base, a poorly-defined diaphragm, and the nasogastric tube in the thoracic base. **c** Enhanced axial CT show the gastric bubble up to the chest. It is difficult to determine whether the finding might be due to eventration of the diaphragm or diaphragmatic reherniation. **d** Coronal and **(b)** sagittal MIP images demonstrate the diaphragmatic hole, through which the stomach has herniated



2011). Furthermore, it is useful for studying congenital lung malformations (pulmonary sequestration, congenital cystic pulmonary airway malformation) (Biyyam et al. 2010), in which depiction of the systemic (aortic feeding) vessel is important for establishing the definitive diagnosis (García-Peña et al. 2013) (Figs. 2, 3, 12, 13, 14).

Cardiac imaging by MDCT is used more frequently in the evaluation of complex congenital pediatric heart diseases (Goo 2011) because of its faster volume coverage and higher

temporal resolution. Retrospective ECG-gated imaging with lower KV and automatic tube current modulation can reduce the effective dose, prospective ECG-gated imaging has been shown to decrease radiation dose to an even greater degree in cardiac CT (Jin et al. 2010; Gao et al. 2012).

The improved contrast enhancement of helical CT and the postprocessing capabilities, such as multiplanar and 3-D reconstructions, are useful for characterizing normal and abnormal vascular anatomy. MRI is usually the technique of

Fig. 27 Intrathoracic rib in an asymptomatic 3-year-old boy. **a** Anteroposterior chest X-ray. There is an abnormal, dense, elongated structure in a right paravertebral position. **b** Axial CT image at the subcarinal level. The dense bony image is seen to arise from the anterior area of the vertebral body. **c** Shaded surface display image better shows the intrathoracic rib with its anterior vertebral origin and its course, running parallel and oblique to the spine

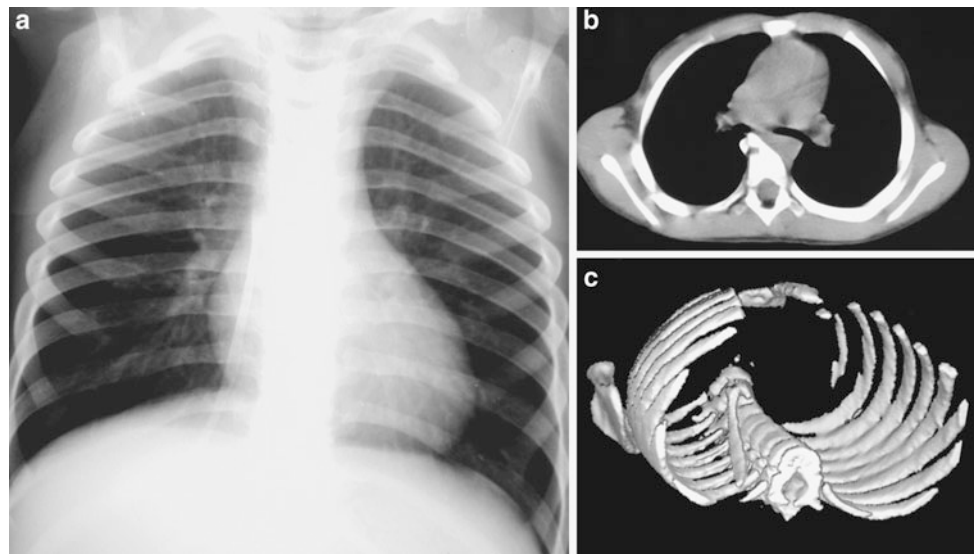
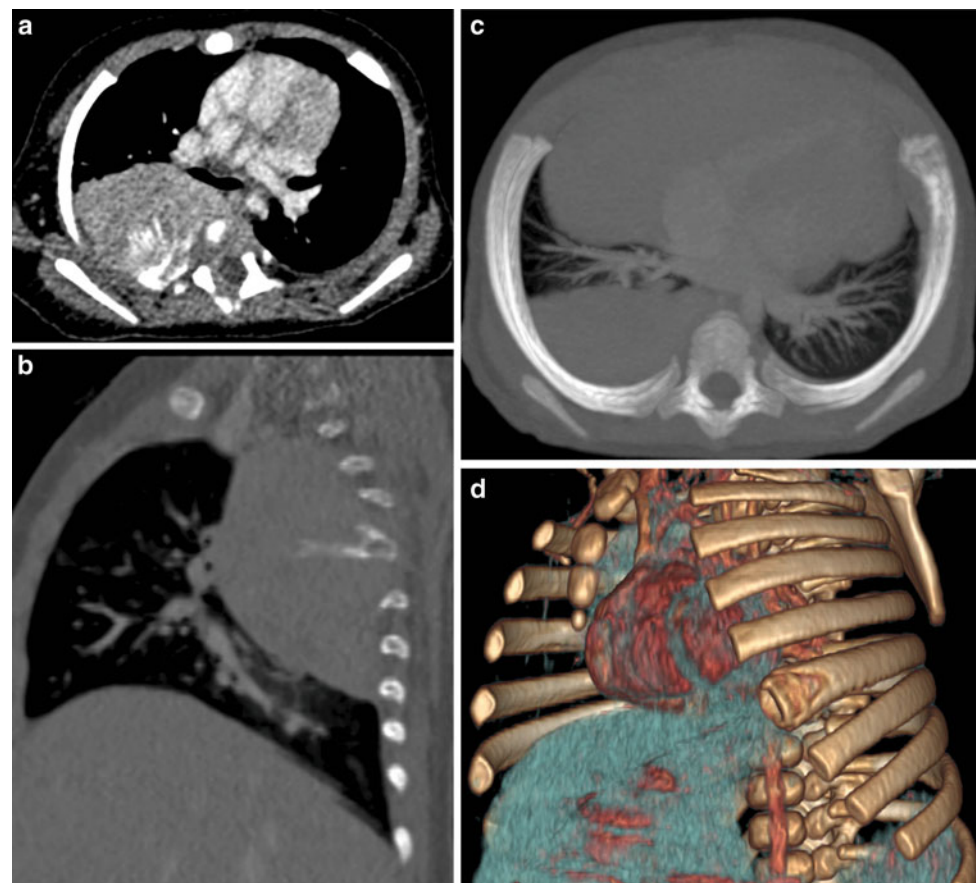


Fig. 28 Metastatic right chest wall PENET with bony invasion in an 11-year-old girl with chest pain. **a** On enhanced axial CT, a mass is seen in the right hemithorax and a bony lesion in the posterior arch of the rib. There is sunrise periosteal reaction. **b** Sagittal MPR shows a long well-defined mass with extrapleural characteristics (“pregnant belly sign”). **c** Axial MIP image, and **d** VRT depict a metastatic bony lesion in the left anterior arch



choice for evaluating congenital large vessel anomalies and other vascular or cardiac anomalies, but helical CT is a feasible alternative in patients whose clinical condition

requires a quick exam and where a lengthy MRI study would not be advisable (Chandrashekar et al. 2012). CT is also invaluable as a one-stop shop when combining vascular

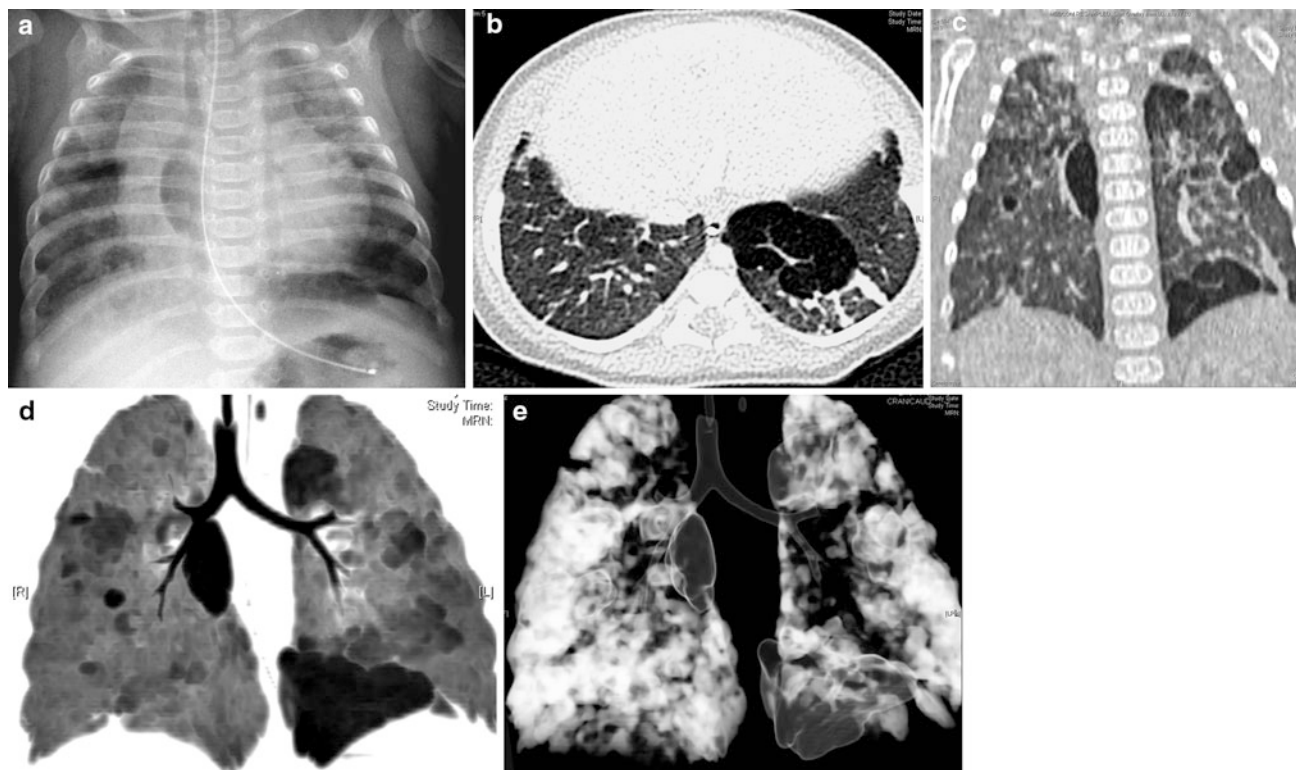


Fig. 29 Inconclusive image on chest X-ray. A preterm neonate who developed respiratory distress soon after birth. **a** Initial chest X-ray shows multiple cystic abnormalities, which are of uncertain aetiology, cystic lung disease, and focal air trapping are the differentials. **b** Axial CT and **c** coronal MPR eloquently confirms the presence of focal air

trapping secondary to respiratory syndrome. The cystic spaces on CXR are seen as areas of segmental air trapping on axial and coronal lung window CT images. **d** MinIP image and **e** VR “bronchogram” volumetric 3D images highlight the hyperlucent areas of the lung and better shows the tracheobronchial tree

and airway abnormalities. Children benefit from the high-speed scan acquisition and the low sedation requirements (Figs. 1, 8, 9, 10).

Several post-processing techniques are available for analysis of the vascular anatomy. Curved multiplanar reconstructions are useful for displaying serpentine vascular structures, such as a systemic vessel in pulmonary sequestration, but they are highly operator-dependent and time-consuming. STS-MIP requires less computer time and can be used as an alternative to curved MPR to improve the depiction of vessels.

MIP, SSD, and VR images, the ones most frequently used to provide information on vascular anatomy, are comparable to conventional angiograms. Since these 3D images can be rotated in a movie loop, they enable visualization of lesions from innumerable viewing angles. This can facilitate analysis of underlying pathologies and improve display of the vessel origin on superimposed images (Figs. 1, 2, 3, 4, 8, 9, 12, 13, 14, 19, 20). Relationships with other important structures (the airways) can also be perceived.

CT angiography can replace conventional angiography in many applications. Helical CT angiocardiology with 3D reconstructions is superior to echocardiography for

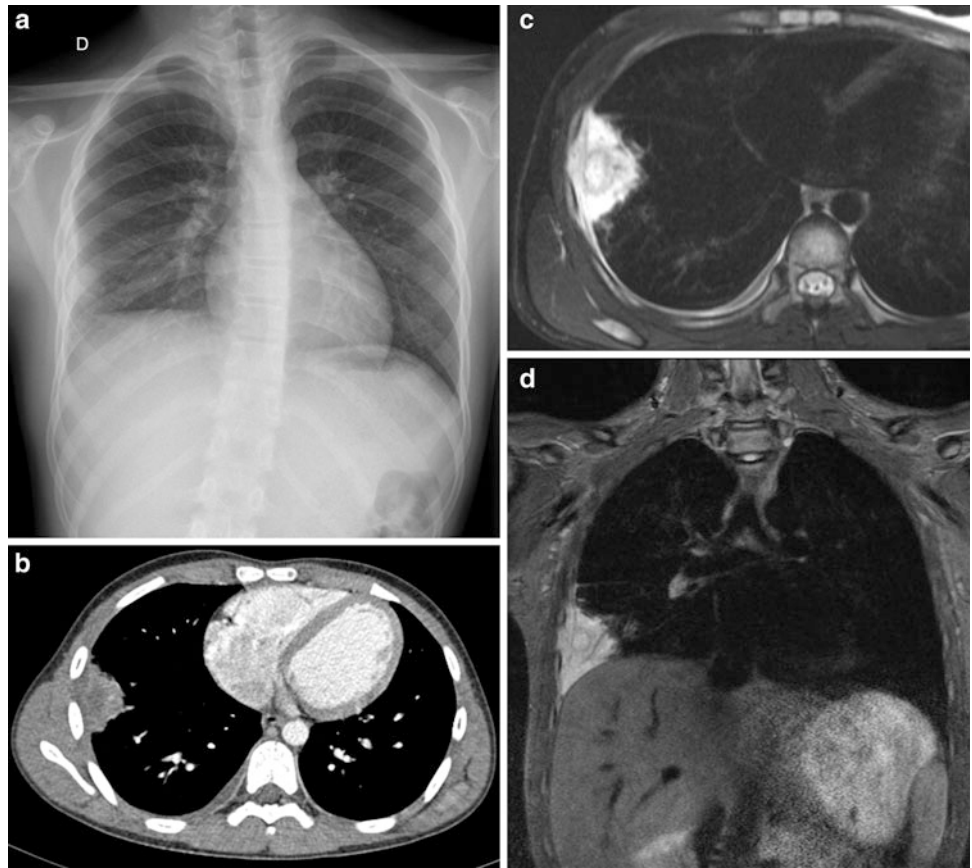
noninvasive assessment of pulmonary artery anatomy and is equal to angiography in patients with complex congenital heart disease (Vestra et al. 1999). As compared to conventional arteriography, CT angiography has the advantages of lower patient morbidity, and reductions in cost and time. Conventional angiography is reserved for angiographic treatment in most cases.

3.3 Evaluation of Central Airways

Helical CT of the central airways is performed with thin collimation during one breath-hold or during quiet respiration (Tables 1 and 2). As a result of the thin-section volumetric scanning, more detailed anatomy can be obtained without partial volume effects. A comparison of standard CT at 8 mm contiguous increment and helical CT with thin collimation and reconstruction at 50 % overlap showed that helical CT was the superior imaging technique (Shafer et al. 1991).

Helical CT demonstrates 95 % of the normal segmental bronchial anatomy. The inferior and superior lingular segmental bronchi, which are often difficult to visualize on conventional CT scans, could be seen in 85 % of patients on helical scans (Costello et al. 1992b). MPR, MIP, SSD, and VR

Fig. 30 Inconclusive images on chest X-ray. A 6-year-old boy with chest pain. Pulmonary abscess was missed on CXR
a Chest X-ray shows a dense longitudinal image vertically following the chest wall, and obliteration of the right costo-diaphragmatic angle. Pleural or chest wall disease was suspected. US shows a mass of difficult localization.
b Enhanced axial CT demonstrates a round peripheral lung lesion with a central hypodensity (abscess), and right pleural thickening. A hypodense area was also visible between the right ribs (small chest wall abscess).
c Axial T2-W FatSat, and **d** Coronal STIR T2-W images show a hyperintense subpleural lung lesion with a hypointense halo area in its center, and a hyperintense lesion going through the ribs on the chest wall. Pleural thickening is also present. *Fusobacterium nucleatum* infection was found in the abscess puncture



images beautifully depict the central airways and are of great clinical value in their assessment (Kauczor et al. 1996; Ferreti et al. 1996; Nicotra et al. 1997; Venkatraman et al. 2006).

Helical CT of the airways is mainly indicated in the study of congenital and acquired abnormalities of the tracheobronchial tree, postpneumectomy complications, complications after lung transplantation, and endobronchial lesions (Berrocal et al. 2004; Kosucu et al. 2004; Choong et al. 2006; Yedururi et al. 2008; Lee et al. 2011; Garcia-Peña et al. 2013) (Figs. 1, 10, 21, 22, 23, 24).

Intensive care and postoperative patients are good candidates for assessment by helical CT. Following pneumectomy, a dehiscence or a bronchopleural fistula can occur at the anastomotic region. Bronchopleural fistula (Fig. 18) is best shown on coronal reformats. Helical CT can demonstrate a bronchopulmonary fistula when conventional axial imaging may be confusing. Two- and three-dimensional images are better than axial images to identify stenotic lesions, especially stenoses in obliquely oriented bronchi. Multiplanar reconstructions along the axis of the bronchus are also useful.

Endobronchial lesions and endobronchial stent location are best shown on multiplanar reconstructions along the axis of the bronchus. Endobronchial lesions (endobronchial tumors, long-standing foreign bodies) can also be shown with virtual endoscopy images (Figs. 22, 24). Intrabronchial

foreign bodies can be difficult to diagnose. There is often no history of foreign body aspiration in children. These patients are usually sent for chest CT examination due to foreign body complications. CT scanning can help in detecting the intrabronchial lesion in these cases.

Helical CT can be useful for evaluating the tracheobronchial tree when using bronchographic images depicted by the VR technique. Tracheobronchography is quite invasive and can carry a significant risk in pediatric patients. This risk is greatest in conditions that compromise the tracheal lumen. Moreover, airway lesions may not be isolated anomalies. It is important to emphasize the possibility offered by helical CT of simultaneously providing bronchographic images and angiographic reconstructions. This combination of data allows evaluation of complex malformations in a single examination and can avoid unnecessary invasive diagnostic procedures (Choo et al. 2006).

Virtual bronchoscopy can be useful for presurgical assessment of strictures that prevent direct passage of a conventional bronchoscope, and for evaluating endoluminal lesions (Honnef et al. 2006) (Figs. 22, 24). Post-processing techniques, such as multiplanar reformatting, volume rendering, and virtual bronchoscopy assist in surgical planning by providing a better representation of 3D anatomy (Yedururi et al. 2008).

MDCT techniques are currently used for noninvasive imaging of patients with suspected tracheobronchomalacia (TBM). Paired end-inspiration, dynamic expiratory MDCT is the examination of choice in these patients (Lee et al. 2009). Dynamic expiratory CT demonstrates a greater degree and extent of airway collapse than standard end-expiratory CT in patients with suspected TBM (Ferretti et al. 2008). Cine CT requires 64-row or greater MDCT scanners, and can be used to rapidly acquire images of the airways throughout the respiratory cycle during free breathing (inspiration and expiration), even in tachypneic patients. In uncooperative patients in whom the controlled-ventilation technique is not feasible, cine CT can be used (Yedururi et al. 2008).

3.4 Evaluation of Difficult Areas: Cervicothoracic Junction, Peridiaphragmatic Area, and Chest Wall

Helical CT is useful for imaging lesions in areas that are difficult to evaluate on axial images and are better assessed on 2- or 3-D reformatted images. Multiplanar reconstructions, generated from helical CT data, are particularly helpful in lesions located in cervicothoracic and apical areas (Fig. 25) (Harty and Kramer 1998), peridiaphragmatic and diaphragmatic areas (Fig. 26) (Brink et al. 1994a; Israel et al. 1996; Chavhan et al. 2010), and the chest wall (Figs. 27, 28) (Donnelly et al. 1997). The reformatted images better depict the extension of lesions and their relationship to adjacent anatomic structures.

Although tumors of the chest wall are uncommon in children, they are often malignant and may aggressively invade the pleural space, lung, spinal canal, or mediastinum. The preoperative imaging evaluation should focus on assessment of the size and extent of the primary tumor and any possible bone invasion or involvement of the chest wall musculature. Both CT and MRI can identify bone and soft-tissue involvement by chest wall tumors (Donnelly et al. 1997). CT is more sensitive in detecting cortical bone disruptions and calcifications, but MRI is better at depicting soft-tissue and marrow involvement. Three-dimensional reconstructions also play a role in the depiction of bony structures of the chest wall and the spine. SSD images can be useful in showing the chest wall deformity in pectus excavatum, but VR images are now used more often for this purpose.

3.5 Evaluation of Critically Ill Patients

One of the greatest advantages of helical CT, especially MDCT, is its speed; examinations are shorter and the need

for sedation is greatly reduced. This means that some patient groups (e.g., very ill patients and trauma cases) who were not previously considered good candidates can now benefit from CT studies (Westra and Wallace 2005). In these patients, the speed of helical CT allows an enormous amount of information to be obtained in a very short time, and enables both the chest and abdomen to be examined with one data acquisition and a single dose of intravenous contrast material. Helical CT studies in these cases should be done under the supervision of the intensive care physician, who also oversees transport of the child to the CT facilities. The images can be reconstructed and reformatted retrospectively after the patient has been returned to the intensive care unit (Veys and Owens 2002; Moore et al. 2011) (Figs. 5, 10, 21).

3.6 Evaluation of Inconclusive Images on Chest Radiography

Helical CT with its technical capabilities of multiplanar and 3D imaging is often useful for defining an inconclusive image seen on chest X-rays and for establishing its exact anatomical location (Figs. 29, 30).

4 Conclusions

Helical CT technology has many potential clinical benefits when used in pediatric patients. These include speed, improved image quality and reductions in the volume of contrast material required, and in the use of sedation. Radiation exposure should be controlled by using low-dose pediatric protocols adjusted to the body weight of the patient, dose modulation techniques, noise reduction systems, and extended pitch when possible, remembering the limitations with automated dose. Two- or three-dimensional reformatted images that are of great value in clinical diagnoses can be generated with the available post-processing methods. The technical aspects of this technique, the clinical indications, and the suggested protocols to be used have been set out in this chapter.

Summary

The increase in radiation burden associated with CT imaging and the potential risk to children cannot be ignored. Therefore, CT requests must be justified with a risk–benefit analysis carried out before undertaking CT examination in children. Imaging techniques and dedicated pediatric protocols must be available to the operators, ensuring adherence to the ALARA principle. The clinical indications have also been set out in this chapter.

References

- Agrons GA, Rosado-de-Christenson ML, Kirejczyk WM et al (1998) Pulmonary inflammatory pseudotumor: radiologic features. *Radiology* 206:511–518
- Ahn MI, Gleeson TG, Chan IH et al (2010) Perifissural nodules seen at CT screening for lung cancer. *Radiology* 254:949
- Ambrosino MM, Genieser NB, Roche KJ et al (1994) Feasibility of high-resolution low-dose chest CT in evaluating the pediatric chest. *Pediatr Radiol* 24:6–10
- Bal CS, Kumar A, Chandra P et al (2004) Is chest X-ray or high-resolution computed tomography scan of the chest sufficient investigation to detect pulmonary metastasis in pediatric differentiated thyroid cancer? *Thyroid* 14:217–225
- Ben Saad M, Rohnan A, Sigal-Cinqualbre A et al (2009) Evaluation of image quality and radiation dose of thoracic and coronary dual-source CT in 110 infants with CHD. *Pediatr Radiol* 39:668–676
- Berrocal T, Madrid C, Novo S et al (2004) Congenital anomalies of tracheobronchial tree, lung, and mediastinum: embryology, radiology, and pathology. *Radiographics* 24:17
- Brenner DJ, Hall EJ (2007) Computed tomography- an increasing source of radiation exposure. *N Engl J Med* 357:2277–2284
- Biyyam DR, Chapman T, Ferguson MR et al (2010) Congenital lung abnormalities: embryologic features, prenatal diagnosis, and postnatal radiologic-pathologic correlation. *Radiographics* 30:1721–1738
- Brink JA (1995) Technical aspects of helical (spiral) CT. *Radiol Clin North Am* 33:825–841
- Brink JA, Heiken JP, Semenkovich J et al (1994a) Abnormalities of the diaphragm and adjacent structures: findings on multiplanar spiral CT scan. *AJR* 163:307–310
- Brink JA, Heiken JP, Wang G et al (1994b) Helical CT: principles and technical considerations. *Radiographics* 14:887–893
- Brody AS, Klein JS, Molina PL et al (2004) High-resolution computed tomography in young patients with cystic fibrosis: distribution of abnormalities and correlation with pulmonary function tests. *J Pediatr* 145:32–38
- Buckley JA, Scott WWJ, Siegelman SS et al (1995) Pulmonary nodules: effect of increased data sampling on detection with spiral CT and confidence in diagnosis. *Radiology* 196:395–400
- Callahan CW (1998) Primary tracheomalacia and gastro-esophageal reflux in infants with cough. *Clin Pediatr (Phila)* 37:725–731
- Chandrashekar G, Sodhi KS, Saxena AK et al (2012) Correlation of 64row MDCT, echography and cardiac catheterization angiography in assessment of pulmonary arterial anatomy in children with congenital heart disease. *Eur J Radiol* 81:4211–4217
- Chavhan GB, Babyn PS, Cohen RA et al (2010) Multimodality imaging of the pediatric diaphragm: anatomy and pathologic conditions. *Radiographics* 30:1797–1817
- Christner JA, Zavaletta VA, Eusemann CD et al (2010) Dose reduction in helical CT: dynamically adjustable z-axis X-ray beam collimation. *Am J Roentgenol* 194:49–55
- Choo KS, Lee HD, Ban JE et al (2006) Evaluation of obstructive airway lesions in complex congenital heart disease using composite volume-rendered images from multi-slice CT. *Pediatr Radiol* 36:219–223
- Choong CK, Sweet SC, Zoole JB (2006) Bronchial airways anastomotic complications after pediatric lung transplantation: incidence, cause, management, and outcome. *J Thorac Cardiovas Surg* 131:198–203
- Chung MP, Yi CA, Lee HY et al (2010) Imaging pulmonary vasculitis. *Radiology* 255:322
- Coakley FV, Cohen MD, Waters DJ et al (1997a) The detection of pulmonary metastases with pathologic correlation in canine model: effect of breathing on the accuracy of helical CT. *AJR* 169:1615–1618
- Coakley FV, Cohen MD, Waters DJ et al (1997b) Detection of pulmonary metastases with pathologic correlation: effects of breathing on accuracy of spiral CT. *Pediatr Radiol* 27:576–579
- Coakley FV, Cohen MD, Johnson MS et al (1998) Maximum intensity projection images in the detection of simulated pulmonary nodules by spiral CT. *Br J Radiol* 71:135–140
- Cohnen M, Vogt C, Beck A et al (2004) Feasibility of MDCT colonography in ultra-low-dose technique in the detection of colorectal lesions: comparison with high-resolution video colonoscopy. *AJR* 183:1355–1359
- Cook BA, Bass JW, Nomizu S, Alexander ME (1992) Sedation of children for technical procedures: current standards of practice. *Clin Pediatr* 31:137–142
- Costello P, Anderson W, Blume D (1991) Pulmonary nodule: evaluation with spiral volumetric CT. *Radiology* 179:875–876
- Costello P, Dupuy DE, Ecker CP et al (1992a) Spiral CT of the thorax with reduced volume of contrast material: a comparative study. *Radiology* 183:663–666
- Costello P, Kruskal J, Dupuy D et al (1992b) Evaluation of tracheobronchial tree with spiral CT. *Radiology* 185:355
- Coursey C, Frush DP, Yoshizumi T et al (2008) Pediatric chest MDCT using tube current modulation: effect on radiation dose with breast shielding. *AJR Am J Roentgenol* 190:54–61
- Dillman JR, Sanchez R, Ladino-Torres MF et al (2011) Expanding upon the unilateral hyperlucent hemothorax in children. *Radiographics* 31:723–741
- Donnelly LF, Taylor CNR, Emery KH et al (1997) Asymptomatic, palpable, anterior chest wall lesions in children: is cross-sectional imaging necessary? *Radiology* 202:829–831
- Egelhoff JC, Ball WS Jr, Kock BL et al (1997) Safety and efficacy of sedation in children using a structured sedation program. *AJR* 168:1259–1262
- Engeler CE, Tashjian JH, Engeler CM (1994) Volumetric high-resolution CT in the diagnosis of interstitial lung disease and bronchiectasis: diagnostic accuracy and radiation dose. *AJR* 163:31–35
- Ferretti GR, Vining DJ, Knoplich J et al (1996) Tracheobronchial tree: three-dimensional spiral CT with bronchoscopic perspective. *J Comput Assist Tomogr* 20:777–781
- Ferretti GR, Jankowski A, Perrin MA et al (2008) Multi-detector CT evaluation in patients suspected of tracheobronchomalacia: comparison of end-expiratory with dynamic expiratory volumetric acquisitions. *Eur J Radiol* 68:340–346
- Frush DP, Donnelly LP (1998) Helical CT in children: technical considerations and body applications. *Radiology* 209:37–48
- Frush DP, Bisett GS III, Hall SC (1996) Pediatric sedation in radiology: the practice of safe sleep. *AJR* 167:1381–1387
- Frush DP, Siegel MJ, Bisett GS III (1997) Challenges of pediatric spiral CT. *Radiographics* 17:939–959
- Frush DP, Slack CC, Hollingsworth CL et al (2002) Computed-simulated radiation dose reduction for abdominal multidetector CT of paediatric patients. *AJR Am J Roentgenol* 179:1107–1113
- Gao Y, Lu B, Hou Z et al (2012) Low-dose dual-source CT angiography in infants with complex congenital heart disease: a randomized study. *Eur J Radiol* 81:e789–e795
- García-Peña P, Lucaya J (2004) High-resolution CT in children, technique and indications. *Eur Radiol* 14:13–20
- García-Peña P, Lucaya J (1999) Chest CT-scan in children: main applications and advantages. *Pediatr Pneumonol* 18:56–59
- García-Peña P, Boixadera H, Barber I et al (2011) Thoracic findings of systemic diseases at high-resolution CT in children. *Radiographics* 31:465–482
- García-Peña P, Coma A, Enriquez G (2013) Congenital lung malformations: radiological findings and clues for the differential diagnosis. *Acta Radiol*. doi:10.1177/0284185113475919

- García-Peña P, Owens CM (2008) Helical multidetector chest CT. In: Lucaya J, Strife JL (2nd eds) *Pediatric chest imaging*. Springer-Verlag Berlin, Heidelberg, pp 47–75
- Gartenschläger M, Schweden F, Gast K et al (1998) Pulmonary nodules: detection with low-dose vs conventional-dose spiral CT. *Eur Radiol* 8:609–614
- Ghersin E, Khoury A, Litmanovich D et al (2005) Comprehensive multidetector computed tomography assessment of severe cardiac contusion in a pediatric patient: correlation with echocardiography. *J Comput Assist Tomogr* 29:739–741
- Goo HW, Seo DM, Yun TJ et al (2009) Coronary artery anomalies and clinically important anatomy in patients with congenital heart disease: multislice CT findings. *Pediatr Radiol* 39:265–273
- Goo HW (2011) Cardiac MDCT in children: CT technology overview and interpretation. *Radiol Clin N Am* 49:997–1010
- Goo HW, Yang DH, Hong SJ et al (2010) Xenon ventilation CT using DS & DE technique in children with bronchiolitis obliterans: correlation of xenon and CT density values with pulmonary function test results. *Pediatr Radiol* 40:1490–1497
- Greess H, Nömayr A, Wolf H et al (2002) Dose reduction in CT examinations of children by an attenuation-based online modulation of tube current (CARE dose). *Eur Radiol* 12:1571–1576
- Greess H, Luzte J, Nömayr A et al (2004) Dose reduction in subsecond multislice spiral CT examination in children by online tube current modulation. *Eur Radiol* 14:995–999
- Gudjónsdóttir J, Ween B, Olsen DR (2010) Optimal use of AEC in CT: a literature review. *Radiol Technol* 81(4):309–317
- Harty MP, Kramer SS (1998) Recent advances in pediatric pulmonary imaging. *Curr Opin Pediatr* 10:227–235
- Heyer CM, Kagel T, Lemburg SP et al (2004) Evaluation of tracheobronchial anomalies in children using low-dose multidetector CT: report of a 13-year-old boy with a tracheal bronchus and recurrent pulmonary infections. *Pediatr Pulmonol* 38:168–173
- Heyer CM, Mohr PS, Lemburg SP et al (2007) Image quality and radiation exposure at pulmonary CT angiography with 100- or 120-kVp protocol: prospective randomized study. *Radiology* 245:577–583
- Hoey ET, Gopalan D, Ganesh V, Agrawal SKB, Qureshi N, Tasker AD, Clements L, Screaton NJ (2009) Dual-energy CT pulmonary angiography: a novel technique for assessing acute and chronic pulmonary thromboembolism. *Clin Radiol* 64:414–419
- Honnef D, Wildberger JE, Das M et al (2006) Value of virtual tracheobronchoscopy and bronchography from 16-slice multidetector-row spiral compute tomography for assessment of suspected tracheobronchial stenosis in children. *Eur Radiol* 16:1684–1691
- Hoppe H, Dinkel HP, Walder B et al (2004) Grading airways stenosis down to the segmental level using virtual bronchoscopy. *Chest* 125:704–711
- Hopper KD, Singapuri K, Finkel A (2000) Body CT and oncologic imaging. *Radiology* 215:27–40
- Hu H, He HD, Foley WD et al (2000) Four multidetector-row helical CT: image quality and volume coverage speed. *Radiology* 215:55–62
- Israel RS, Mayberry JC, Primack SL (1996) Diaphragmatic rupture. Use of helical CT scanning with multiplanar reformations. *AJR* 167:1201–1203
- Jin KN, Park EA, Shin CI et al (2010) Retrospective versus prospective ECG-gated dual-source CT in pediatric patients with congenital heart disease: comparison of image quality and radiation dose. *Int J Cardiovasc Imag* 26:63–73
- Johnson PT, Fishman EK, Duckwall JR et al (1998a) Interactive three-dimensional volume rendering of spiral CT data: current applications in the thorax. *Radiographics* 18:165–187
- Johnson JL, Kramer SS, Mahboubi S (1998b) Air trapping in children: evaluation with dynamic lung densitometry with spiral CT. *Radiology* 206:95–101
- Johnson TRC, Kraub B, Sedlmair M et al (2007) Material differentiation by DECT: initial experience. *Eur Radiol* 17:1510–1517
- Joosten S, MacDonald M, Lau KK et al (2012) Excessive dynamic airway collapse co-morbid with COPD diagnosed using 320-slice dynamic CT scanning technology. *Thorax* 67:95–96
- Kalra MK, Wittram C, Maher MM (2003) Can noise reduction filters improve low-radiation-dose chest CT image? Pilot study. *Radiology* 228:257–264
- Karla MR, Maher MM, Toth TL et al (2004) Comparison of Z-axis automatic tube current modulation technique with fixed tube current CT scanning of abdomen and pelvis. *Radiology* 232:347–353
- Kaste SC, Young CW (1996) Safe use of power injectors with central patient motion and peripheral venous access devices for pediatric CT. *Pediatr Radiol* 26:449–501
- Kaste SC, Young CW, Holmes TP et al (1997) Effect of helical CT on the frequency of sedation in pediatric patients. *AJR* 168:1001–1003
- Katz M, Konen E, Rozenman J, Szeinberg A et al (1995) Spiral CT and 3d image reconstruction of vascular rings and associated tracheobronchial anomalies. *J Comput Assist Tomogr* 19:564–568
- Kauczor HU, Wolcke B, Fisher B et al (1996) Three-dimensional helical CT of the tracheobronchial tree: evaluation of imaging protocols and assessment of suspected stenosis with bronchoscopic correlation. *AJR* 167:419–424
- Kawel N, Seifert B, Luetolf M et al (2009) Effect of slab thickness on the CT detection of pulmonary nodules: use of sliding thin-slab maximum intensity projection and volume rendering. *AJR Am J Roentgenol* 192:1324
- Khan MF, Herzog C, Ackermann H et al (2004) Virtual endoscopy of the trachea-bronchial system: sub-millimeter collimation with 16-row multidetector scanner. *Eur Radiol* 14:1400–1405
- Khandelwal N, Kalra N, Garg MK et al (2011) Multidetector CT angiography in Takayasu arteritis. *Eur J Radiol* 77:S369–S374
- Klusmann M, Owens C (2009) HRCT in paediatric interstitial lung disease—a review for 2009. *Pediatric Radiol* 39:471–481
- Kosucu P, Ahmetoglu A, Koramaz I et al (2004) Low-dose MDCT and virtual bronchoscopy in pediatric patients with foreign body aspiration. *Am J Roentgenol (AJR)* 183:1771–1777
- Kroft LJM, Roelofs JH, Geleijns J (2010) Scan time and patient dose for thoracic imaging in neonates and small children using axial volumetric 320-detector row CT compared to helical 64, 32, and 16 detector row CT acquisition. *Pediatr Radiol* 40:294–300
- Lapierre C, Déry J, Guérin R et al (2010) Segmental approach to imaging of congenital heart disease. *RadioGraphics* 30:397–411
- Lawrence MB (2008) CT angiography in children: is it accurate, but is it safe? *JACC Cardiovasc Imag* 1:340–342
- Lee EY, Greenberg SB, Boiselle PM (2011) Multidetector computed tomography in pediatric large airway diseases: state-of-the-art. *Radiol Clin North Am* 49:869–893
- Lee EY, Litmanovich D, Boiselle PM (2009) Multidetector CT evaluation of tracheobronchomalacia. *Radiol Clin N Am* 47:261–269
- Lee EY, Strauss KJ, Tracy DA et al (2010a) Comparison of standard-dose and reduced-dose expiratory MDCT techniques for assessment of tracheomalacia in children. *Acad Radiol* 17:504–510
- Lee EY, Tracy DA, Bastos M et al (2010b) Expiratory volumetric MDCT evaluation of air trapping in pediatric patients with and without tracheomalacia. *Am J Roentgenol* 194:1210–1215
- Lee EY, Tse SKS, Zarakowski D et al (2012) Children suspected of having pulmonary Embolism: multidetector CT pulmonary angiography-thromboembolic risk factors and implications for appropriated use. *Radiology* 262:242–251
- Lee EY, Zucker EJ, Restrepo R et al (2013) Advances large airway CT imaging in children: evolution from axial to 4-D assessment. *Pediatr Radiol* 43:285–297

- Lobo L, Antunes D (2012) Chest CT in infants and children. *Eur J Radiol*. doi:10.1016/j.ejrad.2011.12.006
- Lucaya J, Decou Le Pointe (2008) High-resolution CT of the lung in children. In: Lucaya J, Strife JL (2nd eds) *Pediatric chest imaging*. Springer-Verlag Berlin, Heidelberg, pp 77–121
- Lucaya J, Garcia-Peña P, Herrera L et al (2000a) Expiratory chest CT in children. *AJR* 174:1–7
- Lucaya J, Piqueras J, Garcia-Peña P et al (2000b) Low-dose high-resolution CT of the chest in children and young adults: dose, cooperation, artifacts incidence, and image quality. *AJR* 175:985–992
- Marini D, Agnoletti G, Brunelle F et al (2009) Cardiac CT angiography after coronary artery surgery in children using 64-slice CT scan. *Eur J Radiol* 71:492–497
- Mc Carville MB, Lederman HM, Santana VM et al (2006) Distinguishing benign from malignant pulmonary nodules with helical CT in children with malignant tumors. *Radiology* 239:514–520
- Mc Hugh K (2008) Chest tumors other than lymphoma. In: Lucaya J, Strife JL (eds) *Pediatric chest imaging*. Chest imaging in infants and children, 2nd edn. Springer, Berlin, Heidelberg, pp 263–287
- Moore MA, Wallace EC, Westra SJ (2011) Chest trauma in children: current imaging guidelines and techniques. *Radiol Clin N Am* 49:949–968
- Napel SA (1995) Basic principles of spiral CT. In: Fishman EK, Jeffrey RB Jr (eds) *Spiral CT: principles, techniques, and clinical application*. Raven, New York, pp 1–9
- Napel SA, Jeffrey RB Jr (1993) STS-MIP: a new reconstruction technique for CT of the chest. *J Comput Assist Tomogr* 17:832–838
- Newman B (2011) Thoracic neoplasms in children. *Radiol Clin N Am* 49:633–664
- Nicotra JJ, Mahboubi S, Kramer SS (1997) Three-dimensional imaging of the pediatric airway. *Int J Pediatr Otorhinolaryngol* 41:299–305
- Oddone M, Granata C, Vercellino N et al (2005) Multi-modality evaluation of the abnormalities of the aortic arches in children: techniques and imaging spectrum with emphasis on MRI. *Pediatr Radiol* 35:947–960
- Ou P, Marini D, Celermajer DS et al (2009) Non-invasive assessment of congenital pulmonary vein stenosis in children using cardiac-gated CT with 64-slices technology. *Eur J Radiol* 70:595–599
- Papaioannou G, Young C, Owens C (2007) Multidetector row CT for imaging the paediatric tracheobronchial tree. *Pediatr Radiol* 37:515–529
- Pappas JN, Donnelly LF, Frush DP (2000) Reduced frequency of sedation of young children with multisection helical CT. *Radiology* 215:897–899
- Paterson A (2005) Imaging evaluation of congenital lung abnormalities in infant and children. *Radiol Clin North Am* 43:303–323
- Paterson A, Frush DP, Donnelly LF (2001) Helical CT of the body: are settings adjusted for pediatric patients? *AJR* 176:1–6
- Pearce MS, Salotti JA, Little MP et al (2012) Radiation exposure from CT scans in childhood and subsequent risk of leukaemia and brain tumours: a retrospective cohort study. *Lancet* 4(380):499–505
- Poole PS and Ferguson EC (2010) Revisiting pulmonary arteriovenous malformations. Radiographic and CT-imaging findings and corresponding treatment options. *Contemporary Diagnostic Imaging (CDR)* 8:1
- Remy-Jardin M, Remy J, Watinne L et al (1992) Central pulmonary thromboembolism: diagnosis with spiral volumetric CT with the single-breath-hold technique comparison with pulmonary angiography. *Radiology* 185:381–387
- Remy-Jardin M, Remi J, Giraud F et al (1993) Pulmonary nodules detection with thick-section spiral CT versus conventional CT. *Radiology* 187:513–520
- Rogalla P, Stöver B, Scheer I et al (1999) Low-dose spiral CT: applicability to paediatric chest imaging. *Pediatr Radiol* 28:565–569
- Rubin GD, Leung AN, Robertson VJ et al (1998) Thoracic spiral CT: influence of subsecond gantry rotation on image quality. *Radiology* 208:771–776
- Saad MB, Rohnean A, Sigal-Cinqualbre A et al (2009) Evaluation of image quality and radiation dose of thoracic and coronary dual-source CT in 110 infants with congenital heart disease. *Pediatr Radiol* 39:668–676
- Sacchetti A, Carraccio C, Giardino A et al (2005) Sedation for pediatric CT scanning: is radiology becoming a drug-free zone? *Pediatr Emerg Care* 21:295–297
- Salvolini L, Bichi SE, Costarelli L et al (2000) Clinical applications of 2D and 3D CT imaging of the airways: a review. *Eur J Radiol* 34:9–25
- Shafer CM, Prokop M, Dohring W et al (1991) Spiral CT of the tracheobronchial system: optimized technique and clinical applications. *Radiology* 181:274
- Shrimpton PC, Edyream S (1998) CT scanner dosimetry. *Br J Radiol* 71:1–3
- Siegel MJ (2003) Multiplanar and three-dimensional multidetector row CT of thoracic vessels and airways in the paediatric population. *Radiology* 229:641–650
- Siegel MJ, Luker GD (1995) Pediatric applications of helical (spiral) CT. *Radiol Clin North Am* 33:997–1022
- Silva AC, Lawder HJ, Hara A et al (2010) Innovations in CT dose reduction strategy: application of the adaptive statistical iterative reconstruction algorithm. *AJR Am J Roentgenol* 194:191–199
- Sillverman PM, Cooper CI, Welman DI et al (1995) Helical CT: practical considerations and potential pitfalls. *Radiographics* 15:25–36
- Singh S, Kalra MK, Shenoy-Bhangle AS, Saini A, Gervais DA, Westra SJ, Thrall JH (2012) Radiation dose reduction with hybrid iterative reconstruction for pediatric CT. *Radiology* 263(2):537–546
- Siripornpitak S, Pornkul R, Khowsathit P et al (2011) Cardiac CT angiography in children with congenital heart disease. *Eur J Radiol*. doi:10.1016/j.ejrad.2011.11.042
- Stokberger SM Jr, Hicklin JA, Liang Y et al (1998) Spiral CT with ionic and non-ionic contrast material: evaluation of patient motion and scan quality. *Radiology* 208:631–636
- Takahashi M, Maguire WM, Ashtari M et al (1998) Low-dose spiral computer tomography of the thorax. *Invest Radiol* 33:68–73
- Trinavarat P (2011) Computed tomographic angiography (CTA) of major thoracic vessels in children. A pictorial essay on common findings also discussing CTA technique. *Eur J Radiol*. doi:10.1016/j.ejrad.2011.12.002
- Turner A, Gavel G, Coutts J (2005) Vascular rings-presentation, investigation and outcome. *Eur J Pediatr* 164:266–270
- Valencia R, Denecke T, Lehmkuhl L et al (2006) Value of axial and coronal maximum intensity projection (MIP) images in the detection of pulmonary nodules by multislice spiral CT: comparison with axial 1-mm and 5 mm slices. *Eur Radiol* 16:325–332
- Venkatraman R, Raman R, Raman B et al (2006) Fully automated system for three-dimensional bronchial morphology analysis using volumetric multidetector Computed tomography of the chest. *J Digit Imag* 19:132–139
- Vestra SJ, Hill JA, Alejos JC et al (1999) Tree-dimensional helical CT of pulmonary arteries in infants and children with congenital heart disease. *AJR* 173:109–115
- Veys P, Owens C (2002) Respiratory infections following haemopoietic stem cell transplantation in children. *Br Med Bull* 61:151–174
- Vyas HV, Greenberg SB, Krishnamurthy R (2012) MR Imaging and CT evaluation of congenital pulmonary vein abnormalities in neonates and infants. *Radiographics* 32:87–98

- Wang G, Vannier MW (1994) Stair-step artifacts in three-dimensional helical CT: an experimental study. *Radiology* 191:79–83
- Westra SJ, Wallace EC (2005) Imaging evaluation of pediatric chest trauma. *Radiol Clin North Am* 43:267–281
- White KS (1995) Reduced need for sedation in patients undergoing helical CT of the chest and abdomen. *Pediatr Radiol* 25:344–346
- Yanagawa M, Honda O, Yoshida S et al (2010) Adaptive statistical iterative reconstruction technique for pulmonary CT: image quality of the cadaveric lung on standard- and reduced-dose CT. *Acad Radiol* 17:1259–1266
- Yedururi S, Guillerman RP, Chung T et al (2008) Multimodality imaging of tracheobronchial disorders in children. *Radiographics*. doi:[10.1148/rg.e29](https://doi.org/10.1148/rg.e29)